
Overexpression of chloroplast-targeted
ferrochelatase 1 results in a *genomes uncoupled*
chloroplast-to-nucleus retrograde signalling
phenotype

Mike Page^{1†}, Tania Garcia-Becerra¹, Alison Smith², Matthew Terry^{1*}

¹School of Biological Sciences, University of Southampton, Highfield
Campus, Southampton SO17 1BJ

²Department of Plant Sciences, University of Cambridge, Cambridge CB2
3EA, UK

Keywords: heme, plastid signalling, tetrapyrroles, mitochondria, *gun* phenotype

Summary

Chloroplast development requires communication between the progenitor plastids and the nucleus, where most of the genes encoding chloroplast proteins reside. Retrograde signals from the chloroplast to the nucleus control the expression of many of these genes, but the signalling pathway is poorly understood. Tetrapyrroles have been strongly implicated as mediators of this signal with the current hypothesis being that heme produced by the activity of ferrochelatase 1 (FC1) is required to promote nuclear gene expression. We have tested this hypothesis by overexpressing FC1 and specifically targeting it to either chloroplasts or mitochondria, two possible locations for this enzyme. Our results show that targeting of FC1 to chloroplasts results in increased expression of the nuclear-encoded chloroplast genes *GUN4*, *CA1*, *HEMA1*, *LHCB2.1*, *CHLH* after treatment with Norflurazon (NF) and that this increase correlates to *FC1* gene expression and heme production measured by feedback inhibition of protochlorophyllide synthesis. Targeting FC1 to mitochondria did not enhance the expression of nuclear-encoded chloroplast genes after NF treatment. Overexpression of FC1 also increased nuclear gene expression in the absence of NF treatment demonstrating that this pathway is operational in the absence of a stress treatment. Our results therefore support the hypothesis that heme synthesis is a promotive chloroplast-to-nucleus

*Author for correspondence (mjt@soton.ac.uk).

†Present address: Lancaster Environment Centre, Lancaster University, Lancaster, LA1 4YQ, UK.

retrograde signal. However, not all FC1 overexpression lines enhanced nuclear gene expression suggesting there is still a lot we do not understand about the role of FC1 in this signalling pathway.

1. Introduction

Chloroplasts evolved through the integration of a free-living photosynthetic prokaryote into a non-photosynthetic eukaryote, followed by relocation of the majority of the chloroplast genome to the nucleus (Jarvis & Lopez-Juez, 2013). The chloroplast retains its own reduced genome, encoding less than 100 predicted proteins in *Arabidopsis thaliana*, with the remaining approximately 3,000 proteins encoded in the nucleus and imported into the developing chloroplast (Abdallah et al., 2000). Consequently, there is a requirement for bidirectional signalling pathways between these organelles to ensure correct provision of proteins to the chloroplast. Anterograde signalling pathways by which the nucleus controls chloroplast development are reasonably well characterized and include photoreceptor and hormone control of nuclear-encoded chloroplast proteins (Jarvis & Lopez-Juez, 2013; Pogson et al., 2015) some of which can control the expression of chloroplast-encoded proteins (Belbin et al., 2017; Yoo et al., 2019). Signalling from the chloroplast to the nucleus during chloroplast development (termed biogenic retrograde signalling; Pogson et al., 2008) is more poorly understood. However, treatments leading to chloroplast damage at the developmental stage results in a strong downregulation of hundreds of nuclear-encoded genes, many encoding chloroplast proteins (Koussevitzky et al., 2007; Woodson et al., 2013). In addition, the impact of the environment on photosynthesis enables chloroplasts to fulfil a sentinel function for environmental stress and various operational retrograde signals from mature chloroplasts can regulate nuclear gene expression to acclimate to these stresses (Pogson et al., 2008; Chan et al., 2016; de Souza et al., 2017).

Our understanding of biogenic retrograde signalling is based on the identification of *genomes uncoupled (gun)* mutants in which expression of the nuclear-encoded *LHCB1.2* gene is maintained after severe chloroplast damage that strongly inhibits expression of many nuclear-encoded photosynthetic genes (Susek et al., 1993). In this case, chloroplast development was prevented by treatment with the phytoene desaturase inhibitor Norflurazon (NF) that blocks the production of photoprotective carotenoids (Breitenbach et al., 2001; Oelmüller et al., 1986). Of the five originally described *gun* mutations, four were in genes encoding proteins required for the synthesis of tetrapyrroles. *gun2* and *gun3* are heme oxygenase and phytychromobilin synthase mutants, respectively, with reduced ability to convert heme to phytychromobilin (Mochizuki et al., 2001). The *gun5* mutation is in the gene encoding the H subunit of Mg-chelatase (Mochizuki et al., 2001) and

gun4 lacks a positive regulator of Mg-chelatase (Larkin et al., 2003). Initial ideas around Mg-protoporphyrin IX (Mg-proto) functioning as a mobile retrograde signal (Strand et al., 2003) have mostly been unsupported as no correlation was observed between Mg-proto levels and *Lhcb* gene expression when Mg-proto levels were manipulated chemically (Moulin et al., 2008) or genetically (Mochizuki et al., 2008). Instead, the identification of the dominant *gun6* mutation that results in elevated ferrochelatase (FC) 1 activity seemed to resolve the *gun* mutant puzzle and led to the hypothesis that synthesis of the FC1 product, heme, was required to promote expression of nuclear-encoded photosynthetic genes (Woodson et al., 2011). As well as making sense of the impact of the *gun* mutations on tetrapyrrole biosynthesis, this hypothesis was consistent with an established role for heme as a signalling molecule in many systems, its relative suitability in terms of its chemistry, and its known export from chloroplasts (Terry and Smith, 2013).

The retrograde signalling field has struggled in recent years with proposed components of the signalling pathway that have not stood up to scrutiny. Recent examples of mutants for which a reported *gun* phenotype has not been reproducible in other laboratories include those lacking PTM1 (Page et al., 2017a) and ABI4 (Kacprzak et al., 2019). However, the phenotypes of the *gun* mutants themselves have been observed in many laboratories over a long period, including the more recently identified *gun6* mutant (Page et al., 2017a). In the current study, we set out to test the hypothesis that FC1 overexpression results in an increase in a promotive retrograde signal, by constructing plants overexpressing FC1. In Arabidopsis (and other higher plants) there are two genes encoding ferrochelatase, *FC1* and *FC2*. The expression profile (Chow et al., 1998; Singh et al., 2002; Moulin et al., 2008; Nagai et al., 2007) and functional analysis (Scharfenberg et al., 2015; Woodson et al., 2015; Espinas et al., 2016; Fan et al., 2019) of these genes is consistent with *FC1* having a role in providing non-photosynthetic heme and *FC2* being required for photosynthetic heme production. For example, mutants lacking FC1 show poor early development with strong alleles being embryo lethal (Espinas et al., 2016; Fan et al., 2019) and reduced accumulation of extra-plastidic cytochromes (Espinas et al., 2016). In contrast, the loss of FC2 results in poor chlorophyll accumulation and reduced development of the photosynthetic apparatus (Scharfenberg et al., 2015; Woodson et al., 2015; Espinas et al., 2016). The *fc2* mutants also show reduced total heme levels. FC2 can partially compensate for the loss of FC1 if expressed from the *FC1* promoter (Fan et al., 2019) and FC1 (with an FC2 transit peptide) can partially compensate the loss of FC2 (Woodson et al., 2015).

There is considerable biochemical evidence that both chloroplasts and mitochondria contain ferrochelatase activity and activity of the preceding enzyme in the pathway, protoporphyrinogen IX

oxidase (Smith et al., 1993; Papenbrock et al., 2001; Cornah et al., 2002; Masuda et al., 2003; Hey et al., 2016). Import experiments in purified organelles also demonstrated that while FC2 was restricted to chloroplasts, FC1 was imported into both chloroplasts and mitochondria, albeit with the majority of FC1 localised in the former (Chow et al., 1997; Suzuki et al., 2002), and recently HA tagged-FC1 was detected in mitochondrial fractions (Hey et al., 2016). These data continue to suggest the possibility of the dual localization of FC1, although some studies do not support this (e.g. Lister et al., 2001). There are links between mitochondria and chloroplasts in retrograde signalling responses (Leister, 2005; Woodson and Chory, 2008; Pfannschmidt, 2010) and it is possible the FC1 may mediate its effect through mitochondrial localization. We have therefore expressed FC1 with its predicted transit peptide replaced with transit peptides specific for plastid (RecA) or mitochondrial import (CoxIV). The RecA and CoxIV transit peptides were selected as they have been used previously to successfully target proteins to these respective organelles (Köhler et al., 1997a,b; Akashi et al., 1998). Our results show that targeting of FC1 to plastids alone is sufficient to promote expression of nuclear-encoded photosynthetic genes and thus our data support the hypothesis that chloroplast-localised FC1 activity is required for retrograde signalling.

2. Materials & methods

(a) Plant material and growth conditions

The *gun5* (Mochizuki et al., 2001) and *gun6* (Woodson et al., 2011) mutants in the Col-0 background have been described previously. For growth on plates, seeds were surface-sterilised with 70% (v/v) ethanol and 10% (v/v) bleach solutions, and plated seeds then imbibed for 3 d at 4 °C in the dark. For selection of transgenics, seeds were plated onto half-strength Murashige and Skoog (MS) medium containing 1% (w/v) agar, pH 5.8, supplemented with 40 µg/mL hygromycin B. For growth of transgenics to determine transgene expression levels, seeds were plated onto half-strength MS medium containing 1% (w/v) agar, pH 5.8. After imbibition, seeds were transferred to WLc (100 µmol m⁻² s⁻¹) at 23 °C for 5 d. For NF screens, seeds were plated onto half-strength Linsmaier and Skoog (LS) medium containing 1% (w/v) sucrose and 1% (w/v) agar, pH 5.8 and supplemented with either 5 µM NF or 0.1% DMSO (control). After imbibition, seeds were transferred to LWLc (25 µmol m⁻² s⁻¹) at 23 °C for 7 d. For growth in soil, seeds were sown directly onto compost (Levington's F2:John Innes No. 2:vermiculite; 1:1:1) and grown in photoperiods of 16 h white light, 8 h dark at 23 °C with a relative humidity of 65%.

(b) Generation of transgenic *Arabidopsis thaliana* lines

The coding sequence of *FC1* was fused at the 3' end to a solubility-modified, red-shifted *GFP* (Akashi et al., 1998), hereafter referred to as *GFP*. A 36 bp spacer was present between the *FC1* sequence and the *GFP* sequence. In addition, the native transit peptide of *FC1* was excluded. This was identified from predictions made using TargetP 1.1 Server (Emanuelsson et al., 2000; Nielsen et al., 1997), predictions of the target peptide cleavage sites based on known cleavage sequences, and alignment of protein sequences to identify amino acids required for function that are conserved across other plant and cyanobacterial species. Following this analysis, the first 77 amino acids of *FC1* (*FC1* Δ^{1-77}) were excluded. A BglII restriction site was added 5' of the *FC1* Δ^{1-77} :*GFP* sequence. The *FC1*:*GFP* fragment was cloned into pDONR™221 (Invitrogen, Carlsbad, USA) using Gateway® technology. A transit peptide conferring localisation either to plastids (*RecA*) or mitochondria (*CoxIV*) was then ligated directly upstream of the gene sequence (at the BglII site) to generate the expression cassettes. The *RecA* transit peptide sequence corresponded to the first 201 bp of the coding sequence of the *Arabidopsis RECA* gene (At1g79050; Cerutti et al., 1992), while the *CoxIV* transit peptide corresponded to the first 87 bp of the coding sequence of cytochrome *c* oxidase subunit 4 from *Saccharomyces cerevisiae* (Maarse et al., 1984). Control expression cassettes lacking *FC1* were also created, consisting of the *GFP* sequence fused downstream of the *RecA* or *CoxIV* transit peptide sequences. Finally, a cassette consisting of the full-length *FC1* (FL-*FC1*) sequence fused to *GFP* was created. The cassettes were recombined into the pGWB502 Ω (hyg^R) plant expression plasmid (Nakagawa et al., 2007) under the control of the 35S promoter from cauliflower mosaic virus, and the resulting plasmids were used to transform *Agrobacterium tumefaciens* GV3101. Flowering *Arabidopsis* Col-0 plants were transformed using the floral dip method (Clough and Bent, 1998), and positive transformants identified through antibiotic selection (Harrison et al., 2006) were confirmed *via* PCR genotyping. Further details on the primers and plasmids used are given in electronic supplementary material Tables S1 and S2, respectively. Plants overexpressing *FC1* targeted to both plastids and mitochondria were generated by manually crossing *CoxIV*:*FC1*:*GFP* lines (female) to *RecA*:*FC1*:*GFP* lines (male).

(c) RNA extraction, cDNA synthesis and qRT-PCR

Cotyledon tissue was homogenised in 500 μ L extraction buffer (100 mM NaCl, 10 mM Tris pH7.0, 1 mM EDTA, 1% (w/v) SDS). After the addition of 150 μ L phenol (pH 4.8), samples were vortexed vigorously. 250 μ L chloroform was then added and the samples again vortexed vigorously. After centrifugation (16,100 x *g*, 5 min, 4°C), the upper aqueous phase was transferred to a new tube

containing 450 μL ice-cold 4 M LiCl. RNA was precipitated overnight at 4°C. After centrifugation (16,100 x g , 20 min, 4 °C), pellets were resuspended in 300 μL DNase buffer (10 mM Tris pH 7.5, 2.5 mM MgCl_2 , 0.5 mM CaCl_2). One μL DNase (Promega, Madison, USA) was then added and samples incubated at 37 °C for 25 min. Samples were mixed with 500 μL phenol:chloroform:isoamyl alcohol (25:24:1), pH 6.7 and vortexed vigorously. After centrifugation (16,100 x g , 5 min, 4 °C), the aqueous upper phase was mixed with 750 μL 95% ethanol:5% 3 M sodium acetate, pH 5.2 and RNA was precipitated at -20 °C for 1 h. After centrifugation (16,100 x g , 20 min, 4 °C), RNA pellets were air dried and resuspended in 50 μL TE buffer (10 mM Tris pH 8.0, 1mM EDTA).

cDNA synthesis was performed according to manufacturer's protocols on 2 μg total RNA per sample with the nanoScript2 kit (Primerdesign, Southampton, UK), using random nonamer and oligo dT primers.

qRT-PCR was carried out on a StepOnePlus™ real-time PCR system (Applied Biosystems, Foster City, USA). Each reaction contained 0.5 μL cDNA, 5 μL PrecisionPLUS SYBR green mastermix (Primerdesign) and 2.5 μL of primer mix (containing forward and reverse primers each at 2 μM), with the volume made up to 10 μL with nuclease-free water. qRT-PCR primer sequences are given in electronic supplementary material Table S3. Two technical replicates were performed for each sample/primer pair combination, and two “no template controls” were performed for each primer pair. qRT-PCR cycling conditions were: 95 °C for 2 min, followed by 40 cycles of 95 °C for 15 s and 60 °C for 1 min, with fluorescence determined at the end of every cycle. Melt curves (60 °C to 92 °C, in 0.5 °C increments) were performed at the end of every run to verify amplification specificity for each primer pair. Primer efficiencies were determined using a serial dilution of Col-0 (untreated) cDNA. Relative expression values between samples were calculated using the $\Delta\Delta\text{Ct}$ method, normalised to *ACTIN DEPOLYMERISING FACTOR 2 (ADF2, At3g46000)* or *YELLOW-LEAF-SPECIFIC GENE 8 (YLS8, At5g08290)*. *ADF2* and *YLS8* were identified as excellent reference genes for NF screens through analysis of microarray data from Col-0 seedlings grown with/without NF (Page et al., 2017b). Data shown was normalised to *ADF2*, with comparable results observed when normalised to *YLS8*. Full details of the qRT-PCR method to fulfil MIQE guidelines (Bustin et al., 2009) are given in electronic supplementary material, datasheet S1.

(d) Chlorophyll, carotenoid and Pchlide determination

Chlorophyll and carotenoids were extracted from weighed cotyledon tissue by homogenising in 800 μL ice-cold 80% (v/v) acetone. After centrifugation (16,100 x g , 5 min, 4 °C), the absorbance of the supernatant was determined at A_{470} , A_{647} and A_{663} using a U-2001 spectrophotometer (Hitachi,

Tokyo, Japan). Total carotenoid and chlorophyll *a* and *b* contents were determined using previously published equations (Lichtenthaler et al., 2001), and normalised to tissue weight.

Pchlide was extracted from cotyledon tissue harvested in a dark room under a dim green safe light using the method described in Terry and Kacprzak (2019). Cotyledon pairs were homogenised in ice-cold acetone:0.1 M ammonium hydroxide (9:1, v:v), centrifuged (16,100 x *g*, 5 min, 4 °C), and fluorescence emission spectra of the supernatants determined (excitation wavelength = 440 nm) using a F-2000 fluorescence spectrophotometer (Hitachi, Tokyo, Japan). The height of the Pchlide peak (~636 nm) was used to generate relative fluorescence values, which were normalised for cotyledon number.

(e) Localization of GFP by confocal imaging

Confocal imaging was used to confirm the subcellular localisation of plastid- and mitochondrion-targeted FC1. Cotyledon tissue from 5 d WLC-grown seedlings was mounted onto slides and the samples flooded with the perfluorocarbon PP11. Localisation of GFP was determined on a Leica TCS SP8 confocal microscope (Leica Microsystems, Wetzlar, Germany), using Leica Application Suite X software. GFP was imaged with an excitation wavelength of 488 nm and detection of emission between 497-531 nm, both using the 63x glycerol oil immersion objective lens. Chlorophyll autofluorescence was detected using 488 nm excitation and 678-695 nm emission. The HyD detector was used to image both signals, and at least 6 averages were taken for each acquisition.

3. Results

(a) Characterisation of FC1 overexpressing lines

We generated transgenic lines containing either a *RecA:FC1:GFP* (plastid-targeted, pFC1) or a *CoxIV:FC1:GFP* (mitochondrion-targeted, mFC1) expression cassette driven by the constitutive CaMV 35S promoter. Selection protocols were used to identify single-insertion, homozygous transformants (T_3 generation) and, subsequently, over-expressing lines were determined by measuring the *FC1* expression level in cotyledon tissue from 5 day old WLC-grown seedlings using qRT-PCR. For the pFC1 lines, expression ranged from 2-fold to 85-fold higher than wild type (WT, Col-0) under these conditions (figure 1a). *FC1* expression levels correlated with *GFP* expression levels from the same plants, while *FC2* expression remained essentially at a WT level (electronic supplementary material, figure S1a). Some of these lines displayed a pale cotyledon phenotype that

appeared to correlate with *FC1* expression, with high over-expressors having very pale cotyledons and low over-expressors being indistinguishable from WT (electronic supplementary material, figure S2a). Control lines over-expressing only *GFP* targeted to plastids, lacked a visible phenotype (electronic supplementary material, figures S1a and S2a). The correlation between the pale cotyledon phenotype and *FC1* expression level was confirmed by analysis of the chlorophyll content of these lines when grown under the same conditions, with the highest over-expressor (pFC1-9) having significantly less total chlorophyll than WT (figure 1c,e). The pFC1-9 line also had significantly less total carotenoids than WT (electronic supplementary material, figure S2b). The next highest over-expressor (pFC1-42) also indicated reductions in chlorophyll and carotenoid content, although these were not statistically significant (figure 1c, electronic supplementary material, figure S2b). *FC1* overexpressing lines using the native transit peptide have previously been reported to have a reduction in chlorophyll synthesis (Woodson et al., 2011). The chlorophyll *a/b* ratio of all pFC1 lines remained similar to WT (electronic supplementary material, figure S2c) and there was no significant effect of day length or light intensity on the accumulation of chlorophyll or carotenoids in these lines (electronic supplementary material, figure S3). Surprisingly, the pale phenotype of pFC1-9 was partially attenuated in mature, soil-grown plants, while the pFC1-42 line showed a paler phenotype compared to seedlings (electronic supplementary material, figure S4).

For the mFC1 lines, *FC1* expression in 5 day old WLC-grown seedlings ranged from 1.2-fold to 20-fold higher than WT (figure 1b). *GFP* expression again correlated with *FC1* expression, with *FC2* expression fundamentally unaffected (electronic supplementary material, figure S1b). No phenotypic differences from WT were observed in these lines at any stage of growth (figure 1d,f, electronic supplementary material, figures S4-6).

Although the paler phenotype of the two transgenic lines pFC1-9 and pFC1-42 correlated quite well with *FC1* expression levels, we wanted to be certain that the observed phenotypes were not due to the insertion site of the *FC1* transgene. We therefore performed whole genome sequencing on both lines to identify the location of the transgenes. As shown in electronic supplementary material, figure S7, the *RecA-FC1-GFP* transgene in pFC1-9 has interrupted the 3' end of At1g01540 at the end of exon 6. All sequence reads indicate that insertion has occurred solely at one location in the genome and confirm our original results from antibiotic selection of T2 seed. At1g01540 is a protein related to Thylakoid-associated kinase 1, but has been determined experimentally to be a cytosolic protein (Armbruster et al., 2009). A GABI-Kat mutant was reported as showing no obvious phenotype (Bölter et al., 2006) and we also obtained independent T-DNA insertion lines for At1g01540 (Salk_008396, Salk_076898 and Salk_036951), but could see no visible loss of greening

phenotype at the seedling stage. For pFC1-42 there was a single insertion site in an intergenic region in chromosome 5 that lies about 600 bp upstream of the start codon of At5g67120 and about 1,250 bp upstream of the start codon of At5g67130. There appears to be up to four T-DNA copies at this single insertion site. At5g67120 and At5g67130 encode an uncharacterised RING/U-box superfamily protein predicted to be nuclear-localised and a plasma membrane localised (Elortza et al., 2006) phospholipase C-like phosphodiesterase superfamily protein with phospholipase activity (Aryal and Lu, 2018), respectively. It is possible that the T-DNA insertion could interfere with the expression of either or both genes, but there is no evidence to suggest this might cause the pFC1-42 phenotype.

(b) Localisation of FC1-GFP proteins

To confirm the localisation of the plastid and mitochondrion-targeted GFP fusion proteins, we examined 5 day old WLC-grown seedlings using confocal imaging. GFP localisation was performed on root tips and cotyledons of the highest over-expressing pFC1 and mFC1 lines. When imaging root tips, GFP labelled structures in cells of pFC1 seedlings were significantly larger than those in mFC1 seedlings (Student's t-test $p < 0.001$, figure 2*a,b*). Moreover, the sizes of the structures in the pFC1 and mFC1 lines closely matched the known sizes of root plastids and mitochondria, respectively (pFC1 = $5.70 \mu\text{m} \pm 0.08$, mFC1 = $1.63 \mu\text{m} \pm 0.12$) (Itoh *et al.*, 2010). In addition, the GFP labelled structures in the mFC1 lines moved rapidly during imaging, supporting the identification of these structures as mitochondria. For lines pFC1-9 and pFC1-42, imaged cotyledons were pale with very few chlorophyll-containing cells (figure 2*a*). GFP was detected in plastids lacking chlorophyll, while no GFP signal was observed when chlorophyll was present. This suggests that the ability to synthesise chlorophyll is an inverse function of plastid *FC1* expression such that high expression of *FC1* protein necessarily limits chlorophyll accumulation. Imaging of mFC1-27 cotyledons further supported mitochondrial localisation of *FC1* in these lines, given the absence of overlap and difference in size between the GFP labelled structures in this line and chloroplasts (figure 2*b*). As expected, a control line in which *GFP* was over-expressed in the absence of a transit peptide showed cytosolic localisation (figure 2*c*).

(c) Retrograde signalling in FC1 overexpressing lines

It was previously demonstrated that over-expression of full-length *FC1* with its native transit peptide rescued the expression of photosynthesis-associated nuclear genes when seedlings were grown on NF (*gun* phenotype) (Woodson et al., 2011). To establish whether organellar-specific over-expression of *FC1* was sufficient to replicate the *gun* phenotype, the transgenic lines described above were grown on NF and expression of nuclear genes determined. *gun5* and *gun6* were included in these screens as positive controls and lines over-expressing *GFP* alone in either plastids (pGFP) or mitochondria (mGFP) were included as negative controls. In the presence of NF, the two highest expressors of plastid-targeted *FC1* (pFC1-9 and pFC1-42) were able to significantly rescue expression of all five nuclear genes tested (*GUN4*, *CA1*, *HEMA1*, *LHCB2.1* and *CHLH*), when compared to Col-0 and pGFP seedlings (figure 3a; electronic supplementary material, figure S8a). In contrast, the highest over-expressing mFC1 lines were not able to rescue the expression of any of the genes tested (figure 3b; electronic supplementary material, figure S8b). Importantly, growth on NF did not have a strong effect on expression of *FC1* in the lines tested (electronic supplementary material, figure S9) and results were independent of the reference gene used (electronic supplementary material, figure S10). Correlation plots of percentage recovery of nuclear gene expression (for all five genes pooled together) after NF treatment *versus* WT and *FC1* expression in the presence of NF show a positive correlation for the plastid-targeted over-expressors (figure 4a), but no correlation for the mitochondrion-targeted over-expressors (electronic supplementary material, figure S11a). These results strongly support the idea that over-expression of *FC1* targeted to plastids is sufficient to rescue expression of nuclear-encoded photosynthesis genes in the presence of NF. Interestingly, both pFC1 and mFC1 lines showed a positive correlation between percentage change in nuclear gene expression and *FC1* expression in the absence of NF (figure 4b; electronic supplementary material, figure S11b), although the maximum increase in expression was just 10% for mFC1 lines compared to 50% for pFC1 lines. The increase in nuclear gene expression observed in pFC1 lines demonstrates the operation of this retrograde pathway under standard plant growth conditions.

Next, we tested whether the effect of elevated plastid *FC1* expression on nuclear gene expression required photoreceptor input in order to be observed. We therefore tested the same five nuclear genes (*GUN4*, *CA1*, *HEMA1*, *LHCB2.1* and *CHLH*) in seedlings grown for 4 d in the dark. In this case, we saw little difference in expression between pFC1 or mFC1 lines and WT for any genes tested (electronic supplementary material, figure S12), except for *HEMA1* expression, which was slightly, yet significantly, increased in pFC1-9 in the dark compared to Col-0 (electronic supplementary

material, figure S12a). An increase in *HEMA1* expression in dark-grown seedlings has previously been noted for *gun1* seedlings (McCormac and Terry, 2004).

To determine if over-expression of FC1 in both organelles would modify the rescue of nuclear gene expression on NF seen in pFC1 lines, pFC1-9 (the highest expressor of plastid-targeted *FC1*) was independently crossed with both mFC1-27 and mFC1-47 (the two highest mitochondrion-targeted *FC1* over-expressors), and the F₁ generation screened on NF. The three parent lines were included in the screens for reference. F₁ plants of both the mFC1-47 x pFC1-9 and mFC1-27 x pFC1-9 lines showed significant enhancement of gene expression after NF treatment (see *CA1* and the tetrapyrrole biosynthesis genes; electronic supplementary material, figure S13a), but expression levels were reduced compared with the pFC1-9 parent line. This was most likely due to the greatly reduced *FC1* expression levels in the F₁ plants compared to the parent lines (electronic supplementary material, figure S13b). The observation that F₁ generation FC1 overexpressing plants can confer a *gun* phenotype demonstrates that this trait is semi-dominant and provides further evidence that the observed phenotype is solely the result of FC1 overexpression.

(d) Modulation of tetrapyrrole synthesis in FC1 over-expressing seedlings correlates with induction of nuclear gene expression

Lines over-expressing plastid-localised *FC1* were able to enhance nuclear gene expression on NF, and this ability correlated with *FC1* expression. To determine if this enhancement of gene expression was due to changes in heme synthesis as proposed by the current model (Woodson et al., 2011; Terry and Smith, 2013), we examined the impact of the overexpressing lines on tetrapyrrole synthesis and determined whether this was also correlated with nuclear gene expression. As it is difficult to measure a signalling heme pool in young seedlings, we determined the accumulation of protochlorophyllide (Pchl_{id}) in the dark as a proxy for such a heme pool at the onset of the light treatment. It is well established that accumulation of heme results in feedback inhibition of aminolevulinic acid (ALA) synthesis resulting in reduced Pchl_{id} (Terry & Kendrick, 1999; Terry et al., 2001; Goslings et al., 2004; Richter et al., 2019). Previous studies have observed elevated Pchl_{id} in *fc2* mutants, but not *fc1* mutants, suggesting that FC2-synthesized heme is responsible for feedback inhibition (Scharfenberg et al., 2015). However, it has been shown that overexpression of FC1 can rescue this phenotype (Woodson et al., 2015) indicating that FC1-synthesized heme can contribute to this regulatory pool. In pFC1 seedlings, Pchl_{id} accumulation in the dark (electronic supplementary material, figure S14) showed a strong negative correlation with expression of all five nuclear genes on NF (figure 5). This correlation was not apparent for mFC1

seedlings (electronic supplementary material, figure S15). Together, these data suggest that there is an elevated regulatory heme pool in pFC1 lines that correlates well with the observed increases in nuclear gene expression in these lines. These results therefore support the hypothesis that increased FC1 activity results in the production of a promotive retrograde signal (Woodson et al., 2011) and, furthermore, that activity in the plastid alone is sufficient for this response.

4. Discussion

The interpretation of the *gun* mutant phenotype has been the focus of our attempts to understand chloroplast-to-nucleus retrograde signalling since these mutants were first described over 25 years ago (Susek et al., 1993). Five of the six *gun* mutants isolated by the Chory laboratory had altered activities of tetrapyrrole biosynthesis-related proteins (Mochizuki et al., 2001; Larkin et al., 2003; Woodson et al., 2011) and the link between tetrapyrrole synthesis and retrograde signalling has stood up to scrutiny over this period. The current hypothesis is that heme synthesized by FC1 is a promotive retrograde signal or precursor of the signal (Woodson et al., 2011; see Terry & Smith 2013; Terry & Bampton 2019; Larkin 2016 for discussion). This hypothesis is based on the observation that both the dominant *gun6* mutation that results in overexpression of *FC1* and a transgenic FC1 overexpression line resulted in enhanced nuclear gene expression after NF treatment and was developed through the re-interpretation of the phenotypes of the *gun2-gun5* mutants (Woodson et al., 2011). Consistent with this hypothesis, heme has a well-established role as a mobile signalling molecule in numerous biological systems (Terry & Smith, 2013). Here we have shown that overexpression of FC1 in chloroplasts results in a strong *gun* phenotype in two independent transgenic lines and that expression of five nuclear-encoded photosynthetic genes correlated with *FC1* gene expression and the ability to feedback inhibit Pchl_{ide} synthesis. Our data therefore broadly support the hypothesis that FC1-dependent heme synthesis results in a promotive chloroplast-to-nucleus retrograde signal. Moreover, this signal is directly related to FC1 activity in the chloroplast as no evidence was observed for a *gun* phenotype when FC1 was targeted to mitochondria. This result is consistent with previous experiments in which overexpression of FC1 using an FC2 transit peptide could increase nuclear gene expression after NF treatment (Woodson et al., 2011), although formally the localization of the FC2-targeted FC1 protein in vivo is unknown as GFP-tagged FC proteins have never been detected in mitochondria despite the strong evidence for the presence of FC in this organelle. Although we were unable to isolate a very highly expressing mFC1 line to match the level of *FC1* over-expression seen in line pFC1-9, under the conditions of the NF screen, three of the mFC1 lines had clearly higher *FC1* expression than pFC1-42, a line that shows significant rescue of nuclear gene expression on NF. Our data do not therefore support a model in

which a chloroplast retrograde signal could have made use of presumably pre-existing mitochondrial signals. Instead, there appears to be direct regulation of nuclear-encoded genes for chloroplast proteins during chloroplast biogenesis.

During the course of this study we identified 6 lines that showed elevated expression of *FC1* in cotyledon tissue under the conditions used for the retrograde signalling assays. Only two of these lines showed a *gun* phenotype, but we included data for all six lines as we wanted to be transparent about the issues we encountered. For example, three of the pFC1 lines (pFC1-22, pFC1-33 and pFC1-48) had similar or higher levels of *FC1* expression on NF than the *gun6* mutant, but did not show a *gun* phenotype and the pFC1-42 and pFC1-48 lines had similarly high *FC1* expression but showed different gene expression responses. This discussion is complicated by the observation that *FC1* expression in *gun6* decreases on NF, something not observed in the overexpression lines. Only pFC1-9 and pFC1-42 showed higher *FC1* expression than *gun6* in the absence of NF and this may account for their ability to confer a *gun* phenotype while other lines were unable to. Importantly perhaps, only these two lines had expression levels that were sufficient to impact on chlorophyll accumulation. Woodson et al (2011) reported reduced chlorophyll levels in all lines that also showed a *gun* phenotype. We are confident that the phenotypes we observed are due to *FC1* overexpression. Genome sequencing to identify the position of each overexpression construct ruled out the likelihood of an insertional effect causing the observed phenotype and the pFC1-9 construct showed a semi-dominant phenotype following crosses with mFC1 lines. Interestingly, even the pFC1-9 and pFC1-42 lines showed slightly different phenotypes with the former showing a stronger reduction in chlorophyll levels in seedlings and the later having a more pronounced mature plant phenotype. This might be related to positional effects altering expression levels in different tissues. Overall, a far more detailed characterization of *FC1* protein levels, localization and activity as well as heme levels for each line would be required to explain the observed phenotypic differences between the different *FC1* overexpressing lines. Nevertheless, we believe our observation that overexpression of *FC1* in chloroplasts can confer a *gun* phenotype, which confirms and builds on the results of Woodson et al (2011), is important in helping to establish an agreed set of reliable data on the retrograde signalling response.

One interesting aspect of our data is the clear demonstration that overexpression of *FC1* resulted in an increase in nuclear gene expression in the absence of NF treatment. Expression of key genes increased up to 50% in pFC1 lines. A small increase was also observed in mFC1 lines although this was not significant for any individual line (electronic supplementary material figure S8). One of the criticisms of the retrograde signalling field is the perceived requirement for severe treatments to

observe the effects of mutations that affect signalling. Our data therefore support the idea that retrograde signalling is functioning under standard growth conditions and that the amount of signal is not necessarily limited. This result therefore supports previous data such as elevated *HEMA1* expression in a *gun1,gun5* double mutant during de-etiolation (McCormac and Terry, 2004).

Finally, a central question in retrograde signalling research is whether single or multiple signals are operating during chloroplast biogenesis. The question derives from analysis of the *gun1* mutation that confers elevated nuclear gene expression after treatments with either NF or the plastid translation inhibitor, lincomycin (Koussevitzky et al., 2007), which has led to the suggestion that GUN1 mediates a signal related to plastid protein synthesis. Indeed, GUN1 does seem to have a role in plastid protein homeostasis (Tadini et al., 2016; Llamas et al., 2017; Marino et al., 2019). However, recently other roles have also been suggested in chloroplast RNA editing (Zhao et al., 2019) and import of nuclear-encoded chloroplast proteins (Wu et al., 2019). GUN1 has also been shown to interact with tetrapyrrole biosynthesis enzymes (Tadini et al., 2016), and to bind heme and a range of porphyrins and regulate FC1 enzyme activity *in vitro* (Shimizu et al., 2019). Given the strong evidence for a tetrapyrrole signal from the heme branch of the pathway, it could be proposed that GUN1 might have a role in co-ordinating various chloroplast processes with production of the FC1-dependent heme signal. Certainly, an understanding of the relationship between GUN1 and FC1-mediated retrograde signalling will be crucial in determining the mechanism of this signalling pathway during chloroplast development.

Acknowledgments

Thanks to Joanne Chory and Jesse Woodson (SALK Institute, USA) for the *gun5* and *gun6* mutants used in this study. Thanks also to George Littlejohn (University of Exeter, UK) for the gift of PP11 and to Chiara Perico and Imogen Sparkes (University of Exeter, UK) for looking at FC1 localization in some of our transgenic lines. M.T.P., T. G-B. and M.J.T. were supported by UK Biotechnology and Biological Sciences Research Council (BBSRC) grant BB/J018139/1. A.G.S. was supported by BBSRC grant BB/J018694/1.

Data accessibility

All datasets supporting this article have been provided as part of the electronic supplementary material.

Authors' Contributions

M.P. performed all of the experiments, analysed data; T. G-B. contributed to making the FC1 overexpressing lines; A.G.S. conceived the project and analysed data. M.J.T. conceived the project and analysed data. All authors contributed to writing the article and approved the final version.

Competing interests

We have no competing interests.

References

- Abdallah F, Salamini F, Leister D. 2000 A prediction of the size and evolutionary origin of the proteome of chloroplasts of *Arabidopsis*. *Trends Plant Sci.* **5**, 141-142. (doi:10.1016/s1360-1385(00)01574-0)
- Akashi K, Grandjean O, Small I. 1998 Potential dual targeting of an *Arabidopsis* archaeobacterial-like histidyl-tRNA synthetase to mitochondria and chloroplasts. *FEBS Lett.* **431**, 39–44. (doi:10.1016/S0014-5793(98)00717-0)
- Armbruster U, Hertle A, Makarenko E, Zuhlke J, Pribil M, Dietzmann A, Schliebner I, Aseeva E, Fenino E, Scharfenberg M, Voigt C, Leister D. 2009 Chloroplast proteins without cleavable transit peptides: rare exceptions or a major constituent of the chloroplast proteome? *Mol. Plant* **2**, 1325-1335. (doi:10.1093/mp/ssp082)
- Aryal N, Lu C. 2018 A phospholipase C-like protein from *Ricinus communis* increases hydroxy fatty acids accumulation in transgenic seeds of *Camelina sativa*. *Front. Plant Sci.* **9**, 1576. (doi:10.3389/fpls.2018.01576)
- Belbin FE, Noordally ZB, Wetherill SJ, Atkins KA, Franklin KA, Dodd AN. 2017 Integration of light and circadian signals that regulate chloroplast transcription by a nuclear-encoded sigma factor. *New Phytol.* **213**, 727–738. (doi:10.1111/nph.14176)
- Bölter B, Nada A, Fulgosi H, Soll J. 2006 A chloroplastic inner envelope membrane protease is essential for plant development. *FEBS Lett.* **580**, 789-794. (doi:10.1016/j.febslet.2005.12.098)

- Breitenbach J, Zhu C, Sandmann G. 2001 Bleaching herbicide norflurazon inhibits phytoene desaturase by competition with the cofactors. *J. Agri. Food Chem.* **49**, 5270-5272. (doi:10.1021/jf0106751)
- Bustin SA, Benes V, Garson JA, Hellemans J, Huggett J, Kubista M, Mueller R, Nolan T, Pfaffl MW, Shipley GL, Vandesompele J, Wittwer CT. 2009 The MIQE guidelines: minimum information for publication of quantitative real-time PCR experiments. *Clin. Chem.* **55**, 611-622. (doi:10.1373/clinchem.2008.112797).
- Cerutti H, Osman M, Grandoni P, Jagendorf AT. 1992 A homolog of *Escherichia coli* RecA protein in plastids of higher plants. *Proc. Natl. Acad. Sci. USA* **89**, 8068–8072. (doi:10.1073/pnas.89.17.8068)
- Chan KX, Phua SY, Crisp P, McQuinn R, Pogson BJ. 2016 Learning the languages of the chloroplast: retrograde signaling and beyond. *Annu. Rev. Plant Biol.* **67**, 25-53. (doi:10.1146/annurev-arplant-043015-111854)
- Chow KS, Singh DP, Roper JM, Smith AG. 1997 A single precursor protein for ferrochelatase-I from *Arabidopsis* is imported *in vitro* into both chloroplasts and mitochondria. *J. Biol. Chem.* **272**, 27565–27571. (doi:10.1074/jbc.272.44.27565)
- Chow KS, Singh DP, Walker AR, Smith AG. 1998 Two different genes encode ferrochelatase in *Arabidopsis*: mapping, expression and subcellular targeting of the precursor proteins. *Plant J.* **15**, 531-541. (doi:10.1046/j.1365-313X.1998.00235)
- Clough SJ, Bent AF. 1998 Floral dip: a simplified method for *Agrobacterium*-mediated transformation of *Arabidopsis thaliana*. *Plant J.* **16**, 735–43. (doi:10.1046/j.1365-313x.1998.00343)
- Cornah JE, Roper JM, Pal Singh D, Smith AG. 2002. Measurement of ferrochelatase activity using a novel assay suggests that plastids are the major site of haem biosynthesis in both photosynthetic and non-photosynthetic cells of pea (*Pisum sativum* L.). *Biochem. J.* **362**, 423-432. (doi:10.1042/bj3620423)
- de Souza A, Wang JZ, Dehesh K. 2017 Retrograde signals: integrators of interorganellar communication and orchestrators of plant development. *Annu. Rev. Plant Biol.* **68**, 85-108. (doi:10.1146/annurev-arplant-042916-041007)
- Elortza F, Mohammed S, Bunkenborg J, Foster LJ, Nühse TS, Brodbeck U, Peck SC, Jensen ON. 2006 Modification-specific proteomics of plasma membrane proteins: identification and characterization

- of glycosylphosphatidylinositol-anchored proteins released upon phospholipase D treatment. *J. Prot. Res.* **5**, 935–943. (doi:10.1021/pr050419u)
- Emanuelsson O, Nielsen H, Brunak S, von Heijne G. 2000 Predicting Subcellular Localization of Proteins Based on their N-terminal Amino Acid Sequence. *J. Mol. Biol.* **300**, 1005–1016. (doi:10.1016/j.cell.2008.06.016)
- Espinás NA, Kobayashi K, Sato Y, Mochizuki N, Takahashi K, Tanaka R, Masuda T. 2016 Allocation of heme is differentially regulated by ferrochelatase isoforms in *Arabidopsis* cells. *Front. Plant Sci.* **7**, 1326. (doi:10.3389/fpls.2016.01326)
- Fan T, Roling L, Meiers A, Brings L, Ortega-Rodés P, Hedtke B, Grimm B. 2019 Complementation studies of the *Arabidopsis fc1* mutant substantiate essential functions of ferrochelatase 1 during embryogenesis and salt stress. *Plant Cell Environ.* **42**, 618–632. (doi:10.1111/pce.13448)
- Goslings D, Meskauskiene R, Kim C, Lee KP, Nater M, Apel K. 2004 Concurrent interactions of heme and FLU with glu tRNA reductase (HEMA1), the target of metabolic feedback inhibition of tetrapyrrole biosynthesis, in dark- and light-grown *Arabidopsis* plants. *Plant J.* **40**, 957–967. (doi:10.1111/j.1365-313X.2004.02262)
- Harrison SJ, Mott EK, Parsley K, Aspinall S, Gray JC, Cottage A. 2006 A rapid and robust method of identifying transformed *Arabidopsis thaliana* seedlings following floral dip transformation. *Plant Methods* **2**, 19. (doi:10.1186/1746-4811-2-19)
- Hey D, Ortega-Rodes P, Fan T, Schnurrer F, Brings L, Hedtke B, Grimm B. 2016 Transgenic tobacco lines expressing sense or antisense *FERROCHELATASE 1* RNA show modified ferrochelatase activity in roots and provide experimental evidence for dual localization of ferrochelatase 1. *Plant Cell Physiol.* **57**, 2576–2585. (doi:10.1093/pcp/pcw171)
- Itoh RD, Yamasaki H, Septiana A, Yoshida S, Fujiwara MT. 2010 Chemical induction of rapid and reversible plastid filamentation in *Arabidopsis thaliana* roots. *Physiol. Plant.* **139**, 144–158. (doi:10.1111/j.1399-3054.2010.01352)
- Jarvis P, López-Juez E. 2013 Biogenesis and homeostasis of chloroplasts and other plastids. *Nat. Rev. Mol. Cell Biol.* **14**, 787–802. (doi:10.1038/nrm3702)

- Kacprzak SM, Mochizuki N, Naranjo B, Xu D, Leister D, Kleine T., Okamoto H, Terry MJ. 2019 Plastid-to-nucleus retrograde signalling during chloroplast biogenesis does not require ABI4. *Plant Physiol.* **179**, 18-23. (doi:10.1104/pp.18.0104)
- Köhler RH, Cao J, Zipfel WR, Webb WW, Hanson MR. 1997a Exchange of protein molecules through connections between higher plant plastids. *Science* **276**, 2039-2042. (doi:10.1126/science.276.5321.2039)
- Köhler RH, Zipfel WR, Webb WW, Hanson MR. 1997b The green fluorescent protein as a marker to visualize plant mitochondria *in vivo*. *Plant J.* **11**, 613-621. (doi:10.1046/j.1365-313X.1997.11030613.x)
- Koussevitzky S, Nott A, Mockler TC, Hong F, Sachetto-Martins G, Surpin M, Lim J, Mittler R, Chory J. 2007 Signals from chloroplasts converge to regulate nuclear gene expression. *Science* **316**, 715-719. (doi:10.1126/science.1140516)
- Larkin RM. 2016 Tetrapyrrole signaling in plants. *Front. Plant Sci.* **7**, 1586. (doi:10.3389/fpls.2016.01586)
- Larkin RM, Alonso JM, Ecker JR, Chory J. 2003 GUN4, a regulator of chlorophyll synthesis and intracellular signaling. *Science* **299**, 902-906. (doi:10.1126/science.1079978)
- Leister D. 2005 Genomics-based dissection of the cross-talk of chloroplasts with the nucleus and mitochondria in *Arabidopsis*. *Gene* **354**, 110–116. (doi:10.1016/j.gene.2005.03.039)
- Lichtenthaler HK, Buschmann C. 2001 Chlorophylls and carotenoids: Measurement and characterization by UV-VIS spectroscopy. *Current Protocols in Food Analytical Chemistry* **1**: F4.3.1–F4.3.8. (doi:10.1002/0471142913.faf0403s01)
- Lister R, Chew O, Rudhe C, Lee MN, Whelan J. 2001 *Arabidopsis thaliana* ferrochelatase-I and -II are not imported into *Arabidopsis* mitochondria. *FEBS Lett.* **506**, 291–295. (doi:10.1016/S0014-5793(01)02925-8)
- Llamas E, Pulido P, Rodriguez-Concepcion M. 2017 Interference with plastome gene expression and Clp protease activity in *Arabidopsis* triggers a chloroplast unfolded protein response to restore protein homeostasis. *PLoS Genet.* **13**, e1007022. (doi:10.1371/journal.pgen.1007022)

Maarse AC, Van Loon AP, Riezman H, Gregor I, Schatz G, Grivell LA. 1984 Subunit IV of yeast cytochrome c oxidase: cloning and nucleotide sequencing of the gene and partial amino acid sequencing of the mature protein. *EMBO J.* **3**, 2831-2837. (doi:10.1002/j.1460-2075.1984.tb02216)

Marino G, Naranjo B, Wang J, Penzler J-F, Kleine T, Leister D. 2019 Relationship of GUN1 to FUG1 in chloroplast protein homeostasis. *Plant J.* **99**, 521-535. (doi:10.1111/tpj.14342)

Masuda T, Suzuki T, Shimada H, Ohta H, Takamiya K. 2003 Subcellular localization of two types of ferrochelatase in cucumber. *Planta* **217**, 602–609. (doi:10.1007/s00425-003-1019-2)

McCormac AC, Terry MJ. 2004 The nuclear genes *Lhcb* and *HEMA1* are differentially sensitive to plastid signals and suggest distinct roles for the GUN1 and GUN5 plastid-signalling pathways during de-etiolation. *Plant J.* **40**, 672–685. (doi:10.1111/j.1365-313X.2004.02243.x)

Mochizuki N, Brusslan JA, Larkin R, Nagatani A, Chory J, 2001 *Arabidopsis genomes uncoupled 5 (GUN5)* mutant reveals the involvement of Mg-chelatase H subunit in plastid-to-nucleus signal transduction. *Proc. Natl. Acad. Sci. USA* **98**, 2053-2058. (doi:10.1073/pnas.98.4.2053)

Mochizuki N, Tanaka R, Tanaka A, Masuda T, Nagatani A. 2008 The steady-state level of Mg-protoporphyrin IX is not a determinant of plastid-to-nucleus signaling in *Arabidopsis*. *Proc. Natl. Acad. Sci. USA* **105**, 15184-15189. (doi:10.1073/pnas.0803245105)

Moulin M, McCormac AC, Terry MJ, Smith AG. 2008 Tetrapyrrole profiling in *Arabidopsis* seedlings reveals that retrograde plastid nuclear signaling is not due to Mg-protoporphyrin IX accumulation. *Proc. Natl. Acad. Sci. USA* **105**, 15178-15183. (doi:10.1073/pnas.0803054105)

Nagai S, Koide M, Takahashi S, Kikuta A, Aono M, Sasaki-Sekimoto Y, Ohta H, Takamiya K-I, Masuda T. 2007 Induction of isoforms of tetrapyrrole biosynthetic enzymes, *AtHEMA2* and *AtFC1*, under stress conditions and their physiological functions in *Arabidopsis*. *Plant Physiol.* **144**, 1039–1051. (doi:10.1104/pp.107.100065)

Nakagawa T, Suzuki T, Murata S, Nakamura S, Hino T, Maeo K, Tabata R, Kawai T, Tanaka K, Niwa Y et al. 2007 Improved Gateway binary vectors: high-performance vectors for creation of fusion constructs in transgenic analysis of plants. *Biosci. Biotech. Biochem.* **71**, 2095–2100. (doi:10.1271/bbb.70216)

- Nielsen H, Engelbrecht J, Brunak S, von Heijne G. 1997 Identification of prokaryotic and eukaryotic signal peptides and prediction of their cleavage sites. *Protein Eng.* **10**, 1–6. (doi:10.1093/protein/10.1.1)
- Oelmüller R, Levitan I, Bergfeld R, Rajasekhar VK, Mohr H. 1986. Expression of nuclear genes as affected by treatments acting on the plastids. *Planta* **168**, 482–492. (doi:10.1007/BF00392267)
- Page MT, Kacprzak SM, Mochizuki N, Okamoto H, Smith AG, Terry MJ. 2017a Seedlings lacking the PTM protein do not show a *genomes uncoupled* (*gun*) mutant phenotype. *Plant Physiol.* **174**, 21–26. (doi:10.1104/pp.16.01930)
- Page MT, McCormac AC, Smith AG, Terry MJ. 2017b Singlet oxygen initiates a plastid signal controlling photosynthetic gene expression. *New Phytol.* **213**, 1168–1180. (doi:10.1111/nph.14223)
- Papenbrock J, Mishra S, Mock HP, Kruse E, Schmidt EK, Petersmann A, Braun HP, Grimm B. 2001 Impaired expression of the plastidic ferrochelatase by antisense RNA synthesis leads to a necrotic phenotype of transformed tobacco plants. *Plant J.* **28**, 41–50. (doi:10.1046/j.1365-313X.2001.01126)
- Pfannschmidt T. 2010 Plastidial retrograde signaling – a true “plastid factor” or just metabolite signatures? *Trends Plant Sci.* **15**, 427–435. (doi:10.1016/j.tplants.2010.05.009)
- Pogson BJ, Ganguly D, Albrecht-Borth V. 2015 Insights into chloroplast biogenesis and development. *Biochim. Biophys. Acta* **1847**, 1017–1024. (doi:10.1016/j.bbabi.2015.02.003)
- Pogson BJ, Woo NS, Förster B, Small ID. 2008 Plastid signalling to the nucleus and beyond. *Trends Plant Sci.* **13**, 602–609. (doi:10.1016/j.tplants.2008.08.008)
- Richter AS, Banse C, Grimm B. 2019 The GluTR-binding protein is the heme-binding factor for feedback control of glutamyl-tRNA reductase. *eLife* **8**, e46300. (doi:10.7554/eLife.46300)
- Scharfenberg M, Mittermayr L, Von Roepenack-Lahaye E, Schlicke H, Grimm B, Leister D, Kleine T. 2015 Functional characterization of the two ferrochelatases in *Arabidopsis thaliana*. *Plant Cell Environ.* **38**, 280–298. (doi:10.1111/pce.12248)
- Shimizu T, Kacprzak SM, Mochizuki N, Nagatani A, Watanabe S, Shimada T, Tanaka K, Hayashi Y, Arai M, Leister D, Okamoto H, Terry MJ, Masuda T. 2019 The retrograde signalling protein GUN1 regulates tetrapyrrole biosynthesis. *Proc. Natl. Acad. Sci. USA* **116**, 24900–24906. (doi:10.1073/pnas.1911251116)

- Singh DP, Cornah JE, Hadingham S, Smith AG. 2002 Expression analysis of the two ferrochelatase genes in *Arabidopsis* in different tissues and under stress conditions reveals their different roles in haem biosynthesis. *Plant Mol. Biol.* **50**, 773–788. (doi:10.1023/A:1019959224271)
- Smith AG, Marsh O, Elder GH. 1993 Investigation of the subcellular location of the tetrapyrrole-biosynthesis enzyme coproporphyrinogen oxidase in higher plants. *Biochem. J.* **292**, 503-508. (doi:10.1042/bj2920503)
- Strand Å, Asami T, Alonso J, Ecker JR, Chory J. 2003 Chloroplast to nucleus communication triggered by accumulation of Mg-protoporphyrinIX. *Nature* **421**, 79-83. (doi:10.1038/nature01204)
- Susek RE, Ausubel FM, Chory J. 1993 Signal transduction mutants of arabidopsis uncouple nuclear *CAB* and *RBCS* gene expression from chloroplast development. *Cell* **74**, 787-799. (doi:10.1016/0092-8674(93)90459-4)
- Suzuki T, Masuda T, Singh DP, Tan FC, Tsuchiya T, Shimada H, Ohta H, Smith AG, Takamiya K. 2002 Two types of ferrochelatase in photosynthetic and nonphotosynthetic tissues of cucumber: their difference in phylogeny, gene expression, and localization. *J. Biol. Chem.* **277**, 4731–4737. (doi:10.1074/jbc.M105613200)
- Tadini L, Pesaresi P, Kleine T, Rossi F, Guljamow A, Sommer F, Mühlhaus T, Schroda M, Masiero S, Pribil M, Rothbart M, Hedtke B, Grimm B, Leister D. 2016 GUN1 controls accumulation of the plastid ribosomal protein S1 at the protein level and interacts with proteins involved in plastid protein homeostasis. *Plant Physiol.* **170**, 1817-1830. (doi:10.1104/pp.15.02033)
- Terry MJ, Bampton J. 2019 The role of tetrapyrroles in chloroplast-to-nucleus retrograde signalling. *Adv. Bot. Res.* **91**, 225-246. (doi:10.1016/bs.abr.2019.05.002)
- Terry MJ, Kacprzak SM. 2019 A simple method for quantification of protochlorophyllide in etiolated *Arabidopsis* seedlings. In *Phytochromes: Methods and Protocols, Methods in Molecular Biology*, vol. 2026. (ed. A Hiltbrunner), pp. 169-177. Springer Nature: New York, USA (doi:10.1007/978-1-4939-9612-4_14)
- Terry MJ, Kendrick RE. 1999 Feedback inhibition of chlorophyll synthesis in the phytochrome chromophore-deficient *aurea* and *yellow-green-2* mutants of tomato. *Plant Physiol.* **119**, 143-152. (doi:10.1104/pp.119.1.143)

Terry MJ, Ryberg M, Raitt CE, Page AM. 2001 Altered etioplast development in phytochrome chromophore-deficient mutants. *Planta* **214**, 314-325. (doi:10.1007/s004250100624)

Terry MJ, Smith AG. 2013 A model for tetrapyrrole synthesis as the primary mechanism for plastid-to-nucleus signaling during chloroplast biogenesis. *Front. Plant Sci.* **4**, 14. (doi:10.3389/fpls.2013.00014)

Woodson JD, Chory J. 2008 Coordination of gene expression between organellar and nuclear genomes. *Nat. Rev. Genet.* **9**, 383-395. (doi:10.1038/nrg2348)

Woodson JD, Joerns MS, Sinson AB, Gilkerson J, Salomé PA, Weigel D, Fitzpatrick JA, Chory J. 2015 Ubiquitin facilitates a quality-control pathway that removes damaged chloroplasts. *Science* **350**, 450-454. (doi: 10.1126/science.aac7444)

Woodson JD, Perez-Ruiz JM, Chory J. 2011 Heme synthesis by plastid ferrochelatase I regulates nuclear gene expression in plants. *Curr. Biol.* **21**, 897-903. (doi:10.1016/j.cub.2011.04.004)

Woodson JD, Perez-Ruiz JM, Schmitz RJ, Ecker JR, Chory J. 2013 Sigma factor-mediated plastid retrograde signals control nuclear gene expression. *Plant J.* **73**, 1–13 (doi:10.1111/tpj.12011)

Wu GZ, Meyer EH, Richter AS, Schuster M, Ling Q, Schöttler MA, Walther D, Zoschke R, Grimm B, Jarvis RP, Bock R. 2019 Control of retrograde signalling by protein import and cytosolic folding stress. *Nat. Plants* **5**, 525-538. (doi:10.1038/s41477-019-0415)

Yoo CY, Pasoreck EK, Wang H, Cao J, Blaha GM, Weigel D, Chen M. 2019 Phytochrome activates the plastid-encoded RNA polymerase for chloroplast biogenesis via nucleus-to-plastid signaling. *Nat. Commun.* **10**, 2629. (doi:10.1038/s41467-019-10518-0)

Zhao X, Huang J, Chory J. 2019 GUN1 interacts with MORF2 to regulate plastid RNA editing during retrograde signalling. *Proc. Natl. Acad. Sci. USA* **116**, 10162-10167. (doi:10.1073/pnas.1820426116)

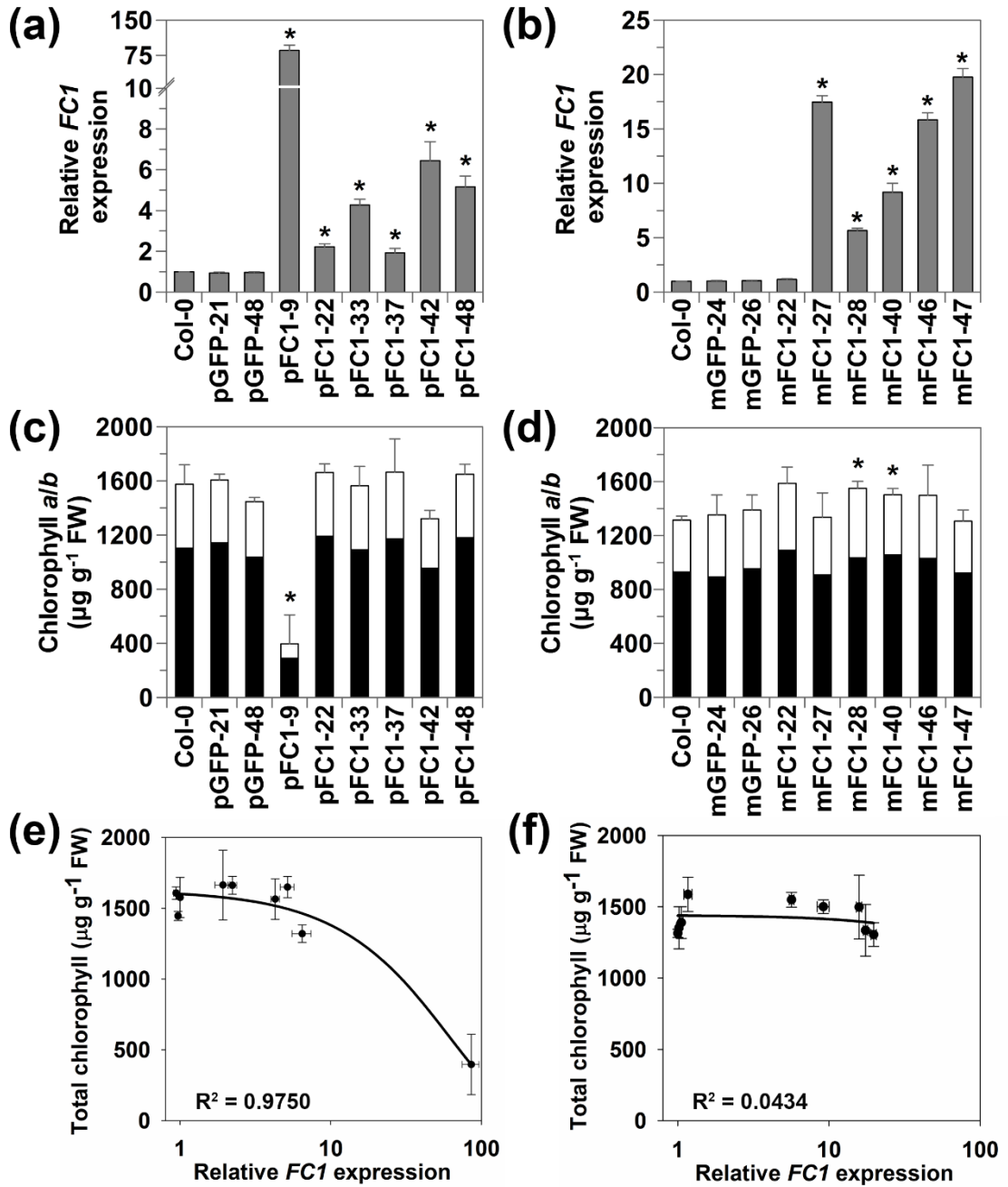


Figure 1. The relationship between *FC1* expression and chlorophyll content in the pFC1 and mFC1 transgenic lines

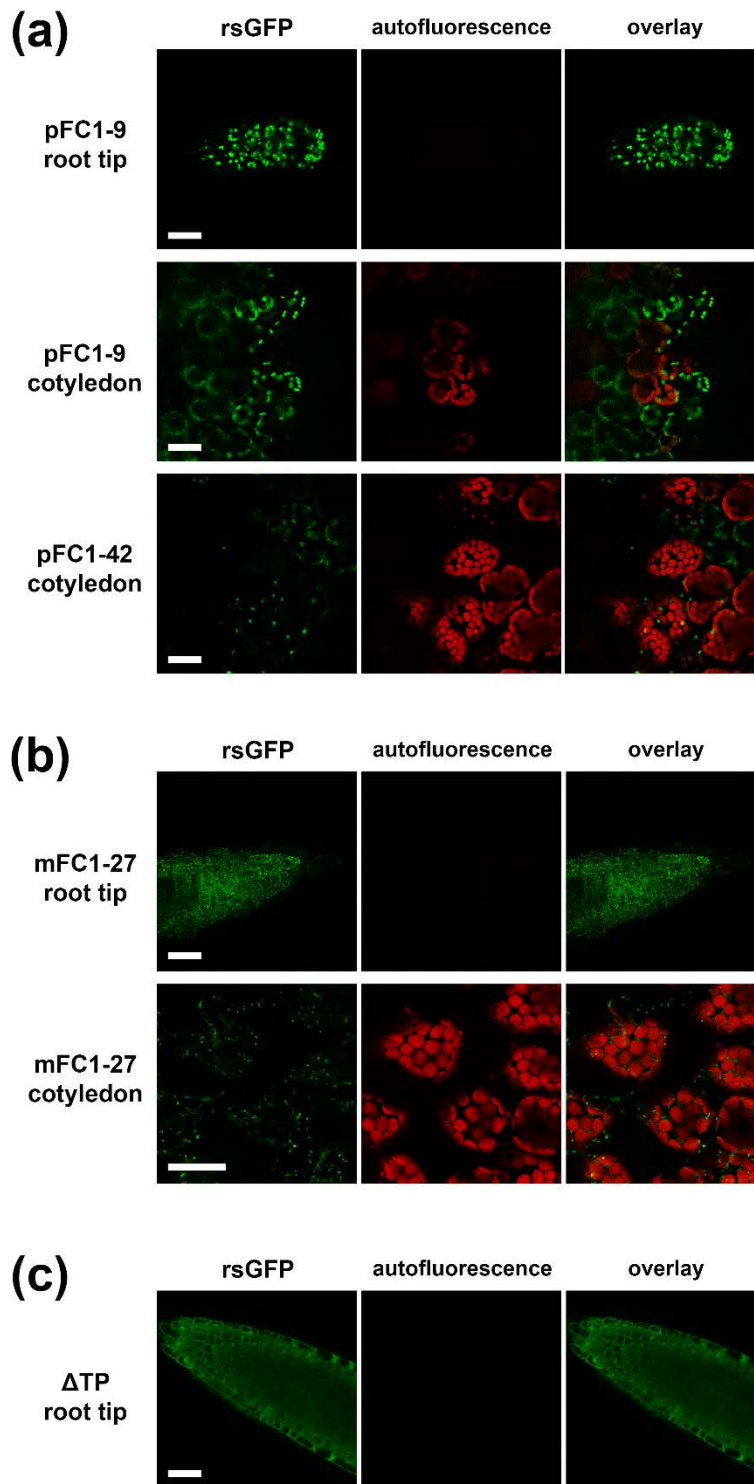


Figure 2. Localisation of FC1 in roots and cotyledons of pFC1 and mFC1 seedlings

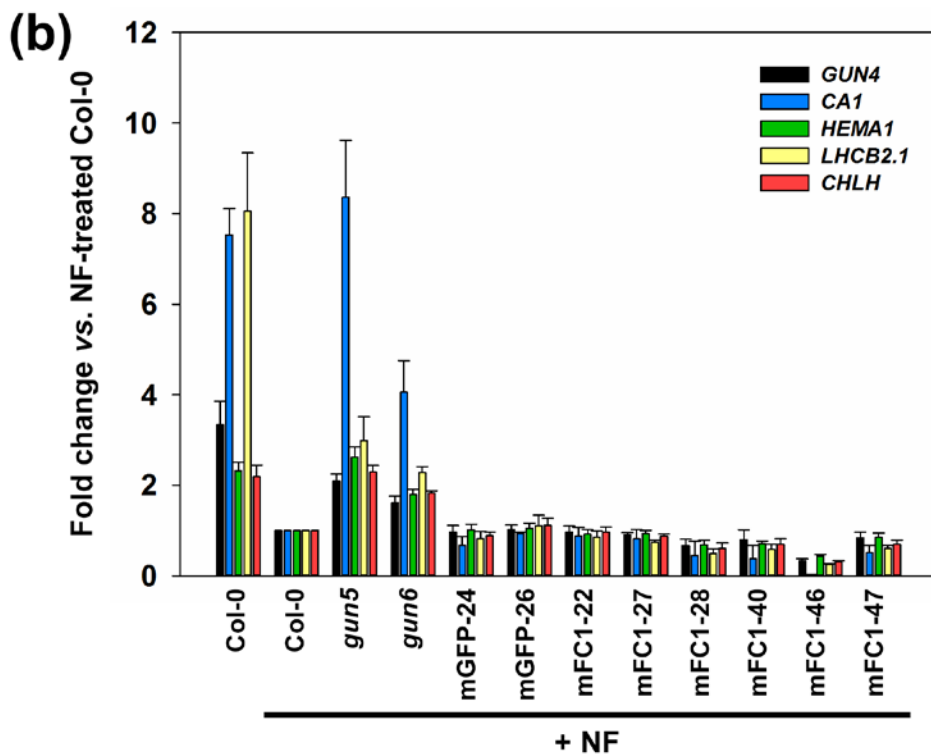
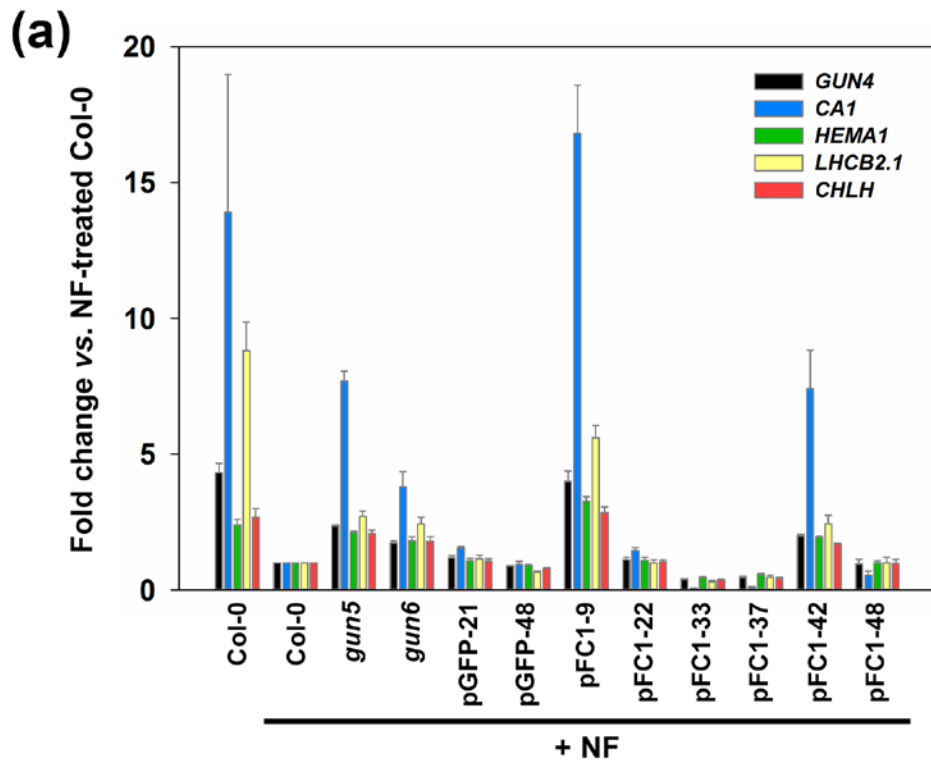


Figure 3. Expression of photosynthesis-associated genes on NF is enhanced in plastid *FC1*, but not mitochondrial *FC1* overexpressors

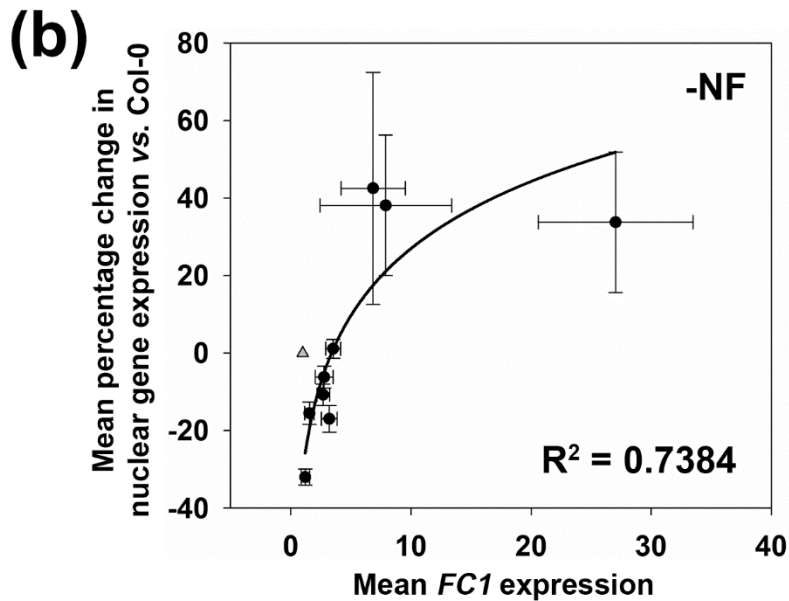
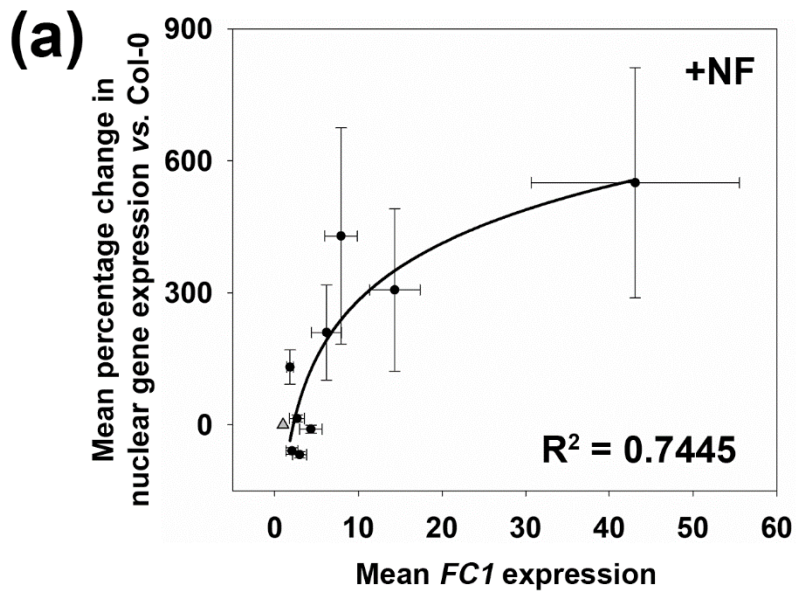


Figure 4. Plastid-targeted *FC1* expression correlates with enhanced nuclear gene expression on NF

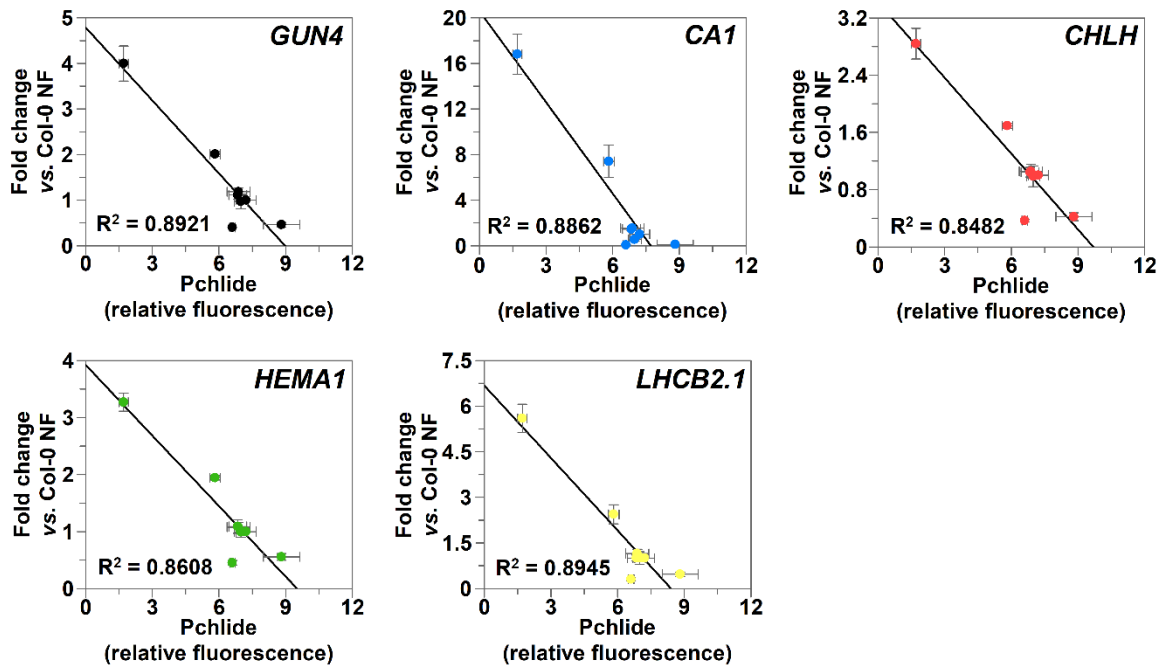


Figure 5. Enhancement of nuclear gene expression on NF inversely correlates with protochlorophyllide levels in dark-grown pFC1 seedlings

Figure legends

Figure 1. The relationship between *FC1* expression and chlorophyll content in the pFC1 and mFC1 transgenic lines. (a,b) *FC1* expression relative to Col-0 in (a) plastid-targeted (pFC1) and (b) mitochondria-targeted (mFC1) *FC1* overexpressing lines as determined by qRT-PCR. (c,d) Total chlorophyll content of the same pFC1 (c) and mFC1 (d) lines. Black bars represent chlorophyll *a* and white bars represent chlorophyll *b*. (e,f) Correlation plots between *FC1* expression (log scale) and total chlorophyll content for the pFC1 (e) and mFC1 (f) lines. Seedlings were grown for 5 d in WLC for all analyses and lines overexpressing only *GFP* in plastids (pGFP) or mitochondria (mGFP) were included as controls. Data represents the mean + SEM of three independent biological replicates and asterisks indicate a significant difference vs. Col-0 ($p < 0.05$, Student's *t*-test).

Figure 2. Localisation of FC1 in roots and cotyledons of pFC1 and mFC1 seedlings. (a,b) Confocal microscopy was used to determine the subcellular localisation of FC1:GFP fusion proteins in pFC1 (a) and mFC1 (b) lines. (c) A control line of FC1:GFP without a transit peptide (Δ TP). Scale bars = 30 μ m.

Figure 3. Expression of photosynthesis-associated genes on NF is enhanced in plastid *FC1*, but not mitochondrial *FC1* overexpressors. (a,b) The expression of *GUN4*, *CA1*, *HEMA1*, *LHCB2.1* and *CHLH* was determined by qRT-PCR in pFC1 (a) and mFC1 (b) seedlings grown for 7 d in LWLC on plates with NF. The control lines pGFP (a) and mGFP (b), as well as *gun5* and *gun6*, were included. Data shown are the mean fold changes vs. Col-0 on NF + SEM of three independent biological replicates. The original qRT-PCR data for these graphs is given in electronic supplementary material figure S8.

Figure 4. Plastid-targeted *FC1* expression correlates with enhanced nuclear gene expression on NF. (a,b) Correlation plots of the combined mean percentage change in expression of *GUN4*, *CA1*, *HEMA1*, *LHCB2.1*, and *CHLH*, vs. *FC1* expression for pFC1 seedlings in the presence (a) or absence (b) of NF. Data is relative to Col-0 +NF (a) or -NF (b). For both graphs, data points include *gun6*, the six transgenic pFC1 overexpressing lines, and two F1 progenies of pFC1 x mFC1 crosses. The triangle indicates WT response. SigmaPlot 13.0 was used to fit logarithmic best-fit lines and derive coefficients of determination. Data shown are the mean \pm SEM of three independent biological replicates.

Figure 5. Enhancement of nuclear gene expression on NF inversely correlates with protochlorophyllide levels in dark-grown pFC1 seedlings. Correlation plots of protochlorophyllide (Pchl) in 4 d-old dark-grown pFC1 seedlings against fold change in expression of *GUN4*, *CA1*, *HEMA1*, *LHCB2.1*, and *CHLH* vs. Col-0 on NF. Data represent the mean \pm SEM of three independent biological replicates.

Electronic Supplementary Material

Table S1. Primers used for molecular cloning of *FC1* and genotyping of transgenic plants.

Table S2. Information on the plasmids used and created during molecular cloning of *FC1*.

Table S3. Information on the primers used for qRT-PCR analysis of gene expression.

Figure S1. Expression of *FC2* and *GFP* in *FC1* overexpressing lines. (a,b) Expression of *FC2* and *GFP* was determined in the same pFC1 (a) and mFC1 (b) seedlings used to generate Figure 1 and is shown relative to Col-0. Lines expressing only *GFP* in plastids (pGFP) or mitochondria (mGFP) were included as controls. Data represents the mean \pm SEM of three independent biological replicates and asterisks indicate a significant difference vs. Col-0 ($p < 0.05$, Student's *t*-test).

Figure S2. Characterisation of 5 day-old WLC-grown seedlings overexpressing plastid-targeted *FC1*. (a) Representative seedling phenotype of pFC1 and pGFP lines, bar = 10 mm. (b) Total carotenoid and (c) chlorophyll *a/b* ratio of the same transgenic lines. For (b, c), data shown is the mean \pm SEM of three independent biological replicates and the asterisk denotes a significant difference vs. Col-0 ($p < 0.05$, Student's *t*-test).

Figure S3. Analysis of chlorophyll and carotenoid levels in pFC1 seedlings grown in different light conditions. (a-d) Total chlorophyll, chlorophyll *a/b* ratio and total carotenoids were measured in pFC1, pGFP (control) and *gun6* 5 d-old seedlings under a range of conditions. (a) LWLc ($25 \mu\text{mol m}^{-2} \text{s}^{-1}$), (b) HWLc ($250 \mu\text{mol m}^{-2} \text{s}^{-1}$), (c) SD (8 h light, 16 h dark, $100 \mu\text{mol m}^{-2} \text{s}^{-1}$), (d) LD (16 h light, 8 h dark, $100 \mu\text{mol m}^{-2} \text{s}^{-1}$). For graphs of chlorophyll content, black bars represent chlorophyll *a* and

white bars represent chlorophyll *b*. Data shown are the mean + SEM of three independent biological replicates and asterisks indicate a significant difference vs. Col-0 ($p < 0.05$, Student's *t*-test).

Figure S4. Phenotype of *FC1* overexpressing lines at the rosette stage. Representative photographs of pGFP, pFC1, mGFP and mFC1 lines. All photographs were taken 23 days after sowing (DAS), except pFC1-9 (34 DAS). Plants were grown on soil in LD conditions (16 h light, 8 h dark, $100 \mu\text{mol m}^{-2} \text{s}^{-1}$), scale bar = 10 mm.

Figure S5. Characterisation of 5 d-old WLC-grown seedlings overexpressing mitochondria-targeted *FC1*. (a) Representative seedling phenotype of mFC1 and mGFP lines, bar = 10 mm. (b) Total carotenoid and (c) chlorophyll *a/b* ratio of the same transgenic lines. For (b) and (c), data shown is the mean + SEM of three independent biological replicates.

Figure S6. Analysis of chlorophyll and carotenoid levels in mFC1 seedlings grown in different light conditions. (a-d) Total chlorophyll, chlorophyll *a/b* ratio and total carotenoids were measured in mFC1, mGFP (control) and *gun6* 5 d-old seedlings under a range of conditions. (a) LWLc ($25 \mu\text{mol m}^{-2} \text{s}^{-1}$), (b) HWLc ($250 \mu\text{mol m}^{-2} \text{s}^{-1}$), (c) SD (8 h light, 16 h dark, $100 \mu\text{mol m}^{-2} \text{s}^{-1}$), (d) LD (16 h light, 8 h dark, $100 \mu\text{mol m}^{-2} \text{s}^{-1}$). For graphs of chlorophyll content, black bars represent chlorophyll *a* and white bars represent chlorophyll *b*. Data shown are the mean + SEM of three independent biological replicates.

Figure S7. Insertion site of transgenic pFC1 cassettes. Diagram to show the insertion site of the transgenic cassette for (a) pFC1-9 and (b) pFC1-42. Exons (yellow boxes) are marked on the full-length genomic DNA sequence (blue boxes). The green line in (a) represents genomic sequence that has been replaced by the insertion. The base pair sizes in (b) give the distance from the insertion site to the start codon of each gene.

Figure S8. Expression of photosynthesis-associated genes on NF is rescued in plastid-targeted, but not mitochondria-targeted, *FC1* overexpressors. (a,b) The expression of *GUN4*, *CA1*, *HEMA1*, *LHCB2.1* and *CHLH* was determined by qRT-PCR in pFC1 (a) and mFC1(b) seedlings grown for 7 d in LWLc on plates in the absence (grey bars) or presence (black bars) of NF. The control lines pGFP (a) and mGFP (b), as well as *gun5* and *gun6*, were included. Data shown are the mean fold changes vs. Col-0 on NF + SEM of three independent biological replicates and asterisks indicate a significant

difference vs. Col-0 ($p < 0.05$, Student's t -test). The data in this figure was used to produce the graphs in Figure 3.

Figure S9. *FC1* expression in pFC1 and mFC1 lines in the NF screen. (a,b) *FC1* expression was determined by qRT-PCR in pFC1 (a) and mFC1 (b) seedlings in the absence (grey bars) or presence (black bars) of NF. Data represents the mean + SEM of three independent biological replicates and asterisks indicate a significant difference vs. Col-0 ($p < 0.05$, Student's t -test).

Figure S10. Gene expression changes on NF in pFC1 seedlings are not dependent on the qRT-PCR reference gene. (a,b) qRT-PCR data shown in electronic supplementary material figures S8 and S9 were normalised to a different reference gene, *YELLOW LEAF SPECIFIC GENE 8* (*YLS8*, At5g08290). The expression of *GUN4*, *CA1*, *HEMA1*, *LHCB2.1*, *CHLH* and *FC1* was determined by qRT-PCR in pFC1 (a) and mFC1(b) seedlings grown for 7 d in LWLc on plates in the absence (grey bars) or presence (black bars) of NF. The control lines pGFP (a) and mGFP (b), as well as *gun5* and *gun6*, were included. Data shown are the mean fold changes vs. Col-0 on NF + SEM of three independent biological replicates and asterisks indicate a significant difference vs. Col-0 ($p < 0.05$, Student's t -test).

Figure S11. Mitochondria-targeted *FC1* expression does not correlate with enhanced nuclear gene expression on NF. Correlation plots of the combined mean percentage change in expression of *GUN4*, *CA1*, *HEMA1*, *LHCB2.1*, and *CHLH*, vs. *FC1* expression for mFC1 seedlings in the presence (a) or absence (b) of NF. Data is relative to Col-0 +NF (a) or -NF (b). For both graphs, data points include *gun6* and the six transgenic *mFC1* overexpressing lines. The triangle indicates WT response. SigmaPlot 13.0 was used to fit logarithmic best-fit lines and derive coefficients of determination. Data shown is the mean \pm SEM of three independent biological replicates.

Figure S12. Increased *FC1* expression does not confer elevated nuclear gene expression in dark-grown seedlings. (a,b) The expression of *GUN4*, *CA1*, *HEMA1*, *LHCB2.1*, *CHLH* and *FC1* was determined by qRT-PCR in pFC1 (a) and mFC1(b) seedlings grown for 4 d in the dark. Data shown is the mean + SEM of three independent biological replicates and asterisks denote a significant difference vs. Col-0 ($p < 0.05$, Student's t -test).

Figure S13. FC1 overexpression in crosses of pFC1 and mFC1 transgenic lines. (a,b) Analysis of gene expression by qRT-PCR in F₁ seedlings derived from a cross between pFC1-9 and mFC1-27, or pFC1-9 and mFC1-47 was assessed in the absence (grey bars) or presence (white bars) of NF by qRT-PCR. The parent lines pFC1-9, mFC1-27 and mFC1-47, as-well-as *gun5* and *gun6*, were included as controls. Expression of *GUN4*, *CA1*, *HEMA1*, *LHCB2.1* and *CHLH* (a) and total, plastid-targeted (*RecA:FC1*) and mitochondria-targeted (*CoxIV:FC1*) *FC1* (b) is shown relative to Col-0. Data shown is the mean \pm range of two independent biological replicates and asterisks denote a significant enhancement of nuclear gene expression vs. Col-0 +NF (determined as no overlap of the 95% confidence limits).

Figure S14. Protochlorophyllide is reduced in pFC1 lines. (a,b) Protochlorophyllide (Pchl) content of pFC1 (a) and mFC1 (b) seedlings grown for 4 d in the dark. Data shown is the mean \pm SEM of three independent biological replicates and asterisks indicate a significant difference in percentage change vs. Col-0 for the same treatment (ANOVA, followed by Tukey's test).

Figure S15. Enhancement of nuclear gene expression on NF does not correlate with protochlorophyllide levels in dark-grown mFC1 seedlings. Correlation plots of protochlorophyllide (Pchl) in 4 d-old dark-grown mFC1 seedlings and against fold change in expression of *GUN4*, *CA1*, *HEMA1*, *LHCB2.1*, and *CHLH* vs. Col-0 on NF. Data represent the mean \pm SEM of three independent biological replicates.

MIQE checklist

Supplementary material for Phil. Trans. R. Soc. B. article

Overexpression of chloroplast-targeted ferrochelatase 1
results in a *genomes uncoupled* chloroplast-to-nucleus
retrograde signalling phenotype

Mike Page¹, Tania Garcia-Becerra¹, Alison Smith², Matthew Terry¹

**¹School of Biological Sciences, University of Southampton, Highfield
Campus, Southampton SO17 1BJ**

**²Department of Plant Sciences, University of Cambridge, Cambridge
CB2 3EA, UK**

Table S1. Primers used for molecular cloning of *FC1* and genotyping of transgenic plants.

Reaction	Purpose	Primer	Primer sequences (5' > 3')
1	Amplification of <i>FC1:spGFP</i> , to remove the native FC1 transit peptide and add a BglIII restriction site at the 5' end of the amplicon.	A	<u>AGATCT</u> GCTAAAGCACGTTCTCATG
		B	GCTCTTATTTGTATAGTTCATCCATGC
2	Re-amplification of the amplicon obtained in reaction 1, to add <i>attB</i> Gateway® recombination sites at each end (step 1 of a two-step reaction).	C	<u>AAAAGCAGGCTCA</u> <u>AGATCT</u> GCTAAAGCAC
		D	<u>GAAAGCTGGGCT</u> TTATTTGTATAGTTCATCC
3	Re-amplification of the amplicon obtained in reaction 1, to add <i>attB</i> Gateway® recombination sites at each end (step 2 of a two-step reaction).	E	<u>GGGGACAAGTTTGTACAAAAAAGCAGGCT</u>
		F	<u>GGGGACCACTTTGTACAAGAAAGCTGGGT</u>
4	Amplification of the RecA transit peptide, to add BglIII restriction sites at both ends of the amplicon.	G	<u>AGATCT</u> ATGGATTCACAGCTAGTCTTG
		H	<u>AGATCT</u> TCTGTCATCGAATTCAGAAC
5	Amplification of the CoxIV transit peptide, to add BglIII restriction sites at both ends of the amplicon.	I	<u>AGATCT</u> ATGCTTTCACCTACGCTCAATCT
		J	<u>AGATCT</u> GGGTTTTTGTCTGAAGCAGA
6	Amplification of <i>RecA:spGFP</i> , to add <i>attB</i> Gateway® recombination sites at each end (step 1 of a two-step reaction).	K	<u>AAAAGCAGGCTAC</u> ATGGATTCACAGCTAG
		D	<u>GAAAGCTGGGCT</u> TTATTTGTATAGTTCATCC
7	Amplification of <i>RecA:spGFP</i> from the amplicon obtained in reaction 6, to add <i>attB</i> Gateway® recombination sites at each end (step 2 of a two-step reaction).	E	<u>GGGGACAAGTTTGTACAAAAAAGCAGGCT</u>
		F	<u>GGGGACCACTTTGTACAAGAAAGCTGGGT</u>
8	Amplification of <i>CoxIV:spGFP</i> , to add <i>attB</i> Gateway® recombination sites at each end (step 1 of a two-step reaction).	L	<u>AAAAGCAGGCTAC</u> ATGGTTTCACTACGTC
		D	<u>GAAAGCTGGGCT</u> TTATTTGTATAGTTCATCC
9	Amplification of <i>CoxIV:spGFP</i> from the amplicon obtained in reaction 8, to add <i>attB</i> Gateway® recombination sites at each end (step 2 of a two-step reaction).	E	<u>GGGGACAAGTTTGTACAAAAAAGCAGGCT</u>
		F	<u>GGGGACCACTTTGTACAAGAAAGCTGGGT</u>
10	Amplification of the full-length <i>FC1</i> coding sequence (FL- <i>FC1</i>) fused to <i>GFP</i> , to add <i>attB</i> Gateway® recombination sites at each end (step 1 of a two-step reaction).	M	<u>AAAAGCAGGCTCA</u> ATGCAGGCAACGG
		D	<u>GAAAGCTGGGCT</u> TTATTTGTATAGTTCATCC
11	Amplification of FL- <i>FC1</i> fused to <i>GFP</i> from the amplicon obtained in reaction 10, to add <i>attB</i> Gateway® recombination sites at each end (step 2 of a two-step reaction).	E	<u>GGGGACAAGTTTGTACAAAAAAGCAGGCT</u>
		F	<u>GGGGACCACTTTGTACAAGAAAGCTGGGT</u>
12	Genotyping <i>RecA:FC1:GFP</i> transgenic lines. Product size = 560 bp.	N	GGATTCACAGCTAGTCTTGTCTCTG
		O	CCTCCTCAGTGAACGGATACC
13	Genotyping <i>CoxIV:FC1:GFP</i> transgenic lines. Product size = 416 bp.	P	CAAGCCAGCCACAAGAACCTTG
		O	CCTCCTCAGTGAACGGATACC
14	Genotyping <i>RecA:GFP</i> and <i>CoxIV:GFP</i> transgenic lines. Product sizes = 447 bp and 330 bp respectively.	Q	GGATGACGCACAATCCCACATATC
		R	CAAGAATTGGGACAACCTCCAG
15	Genotyping FL- <i>FC1:GFP</i> transgenic lines. Product size = 783 bp.	Q	GGATGACGCACAATCCCACATATC
		O	CCTCCTCAGTGAACGGATACC

Restriction enzyme recognition sites within primer sequences are given in blue text. Gateway® *att* recombination sequences (including any extra bases to maintain reading frames) within primers are underlined.

Table S2. Information on the plasmids used and created during molecular cloning of *FC1*.

Plasmid name	Insert name	Parent plasmid/ amplicon	<i>Arabidopsis</i> lines	Notes	Reference
pGEM®-T Easy				TA cloning plasmid (Amp ^R).	Promega
pDONR™221				Gateway® cloning plasmid (Kan ^R).	Invitrogen™
pGWB502Ω				Gateway® destination plasmid (Spec ^R). The plant selectable marker is hygromycin.	Nakagawa <i>et al</i> (2007)
pGEM®-T FC1-GFP	<i>FC1:GFP</i>	pGEM®-T Easy & reaction 1		Subcloning of <i>FC1:GFP</i> (no native transit peptide).	
pENTR FC1-GFP	<i>FC1:GFP</i>	pDONR™221 & reaction 3		Cloning <i>FC1:GFP</i> (no native transit peptide) into a Gateway® plasmid.	
pGEM®-T RecA	<i>RecA</i>	pGEM®-T Easy & reaction 4		Subcloning of <i>RecA</i> transit peptide.	
pGEM®-T CoxIV	<i>CoxIV</i>	pGEM®-T Easy & reaction 5		Subcloning of <i>CoxIV</i> transit peptide.	
pENTR RecA-FC1-GFP	<i>RecA:FC1:GFP</i>	pENTR FC1-GFP & pGEM®-T RecA (BglII digest)		Ligation of <i>RecA</i> transit peptide upstream of <i>FC1:GFP</i> .	
pENTR CoxIV-FC1-GFP	<i>CoxIV:FC1:GFP</i>	pENTR FC1-GFP & pGEM®-T CoxIV (BglII digest)		Ligation of <i>CoxIV</i> transit peptide upstream of <i>FC1:GFP</i> .	
pGWB502Ω RecA-FC1-GFP	<i>RecA:FC1:GFP</i>	pENTR RecA-FC1-GFP & pGWB502Ω	pFC1	Recombination of <i>RecA:FC1:GFP</i> into a destination plasmid.	
pGWB502Ω CoxIV-FC1-GFP	<i>CoxIV:FC1:GFP</i>	pENTR CoxIV-FC1-GFP & pGWB502Ω	mFC1	Recombination of <i>CoxIV:FC1:GFP</i> into a destination plasmid.	
pENTR RecA-GFP	<i>RecA:GFP</i>	pDONR™221 & reaction 7		Cloning <i>RecA:GFP</i> into a Gateway® plasmid.	
pGWB502Ω RecA-GFP	<i>RecA:GFP</i>	pENTR RecA-GFP & pGWB502Ω	pGFP	Recombination of <i>RecA:GFP</i> into a destination plasmid.	
pENTR CoxIV-GFP	<i>CoxIV:GFP</i>	pDONR™221 & reaction 9		Cloning <i>CoxIV:GFP</i> into a Gateway® plasmid.	
pGWB502Ω CoxIV-GFP	<i>CoxIV:GFP</i>	pENTR CoxIV-GFP & pGWB502Ω	mGFP	Recombination of <i>CoxIV:GFP</i> into a destination plasmid.	
pENTR FL-FC1-GFP	<i>FL-FC1:GFP</i>	pDONR221™ & reaction 11		Cloning <i>FL-FC1:GFP</i> into a Gateway® plasmid.	
pGWB502Ω FL-FC1-GFP	<i>FL-FC1:GFP</i>	pENTR FL-FC1-GFP & pGWB502Ω	FLFC1	Recombination of <i>FL-FC1:GFP</i> into a destination plasmid.	

The reactions referred to in column three relate to the amplicons created in the reactions described in Supplementary Table S1.

Table S3. Information on the primers used for qRT-PCR analysis of gene expression.

Gene name	Accession No. (source)	Forward primer sequence (5' > 3')	Reverse primer sequence (5' > 3')	Amplicon length (bp)
<i>FC1</i>	At5g26030 (TAIR)	CCTGAACTCTTAACGATGTTTC	CCACCAATAGCAGCATAACC	164
<i>GFP</i>	U70496.1 (GenBank)	GAGGACCATCTCTTCAAGGAC	GTTGTGGGAGTTGTAGTTGTATTC	163
<i>FC2</i>	At2g30390 (TAIR)	GCAGAGATGGAAGAATGTGTTG	CAGTAATGGCTTCTTCAGTGATG	139
<i>ADF2</i>	At3g46000 (TAIR)	CGATTTGACTTTGTCCTGTC	TCATCTTGTCTCTCACTTTGGC	95
<i>YLS8</i>	At5g08290 (TAIR)	GCTGAAATATCCCGTGAAGTGC	AATGGAGAACAACCGAAACAG	93
<i>GUN4</i>	At3g59400 (TAIR)	CAATCTCACTTCGGACCAAC	TTGAAACGGCAGATACGG	121
<i>CA1</i>	At3g01500 (TAIR)	GCTTCTTTCTCACTTCACTTTCTC	CAATGATAGGAGCAGGAGCG	189
<i>HEMA1</i>	At1g58290 (TAIR)	GCTTCTTCTGATTCTGCGTC	GCTGTGTGAATACTAAGTCCAATC	128
<i>LHCB2*1</i>	At2g05100 (TAIR)	CTCCGCAAGGTTGGTGTATC	CGGTTAGGTAGGACGGTGTAT	142
<i>CHLH</i>	At5g13630 (TAIR)	CATTGCTGACACTACAAGTGC	CTTCTCTATCTCACGAAGTCTTTC	145
<i>RecA:FC1</i>	Created in this study	CTTCACTCTCTTTCTCTCTCT	CAACAACATGAGAACGTGCTTTA	191
<i>CoxIV:FC1</i>	Created in this study	CAAGCCAGCCACAAGAAGTCT	CATCGTTAAGAGTTTCAGGACCA	146

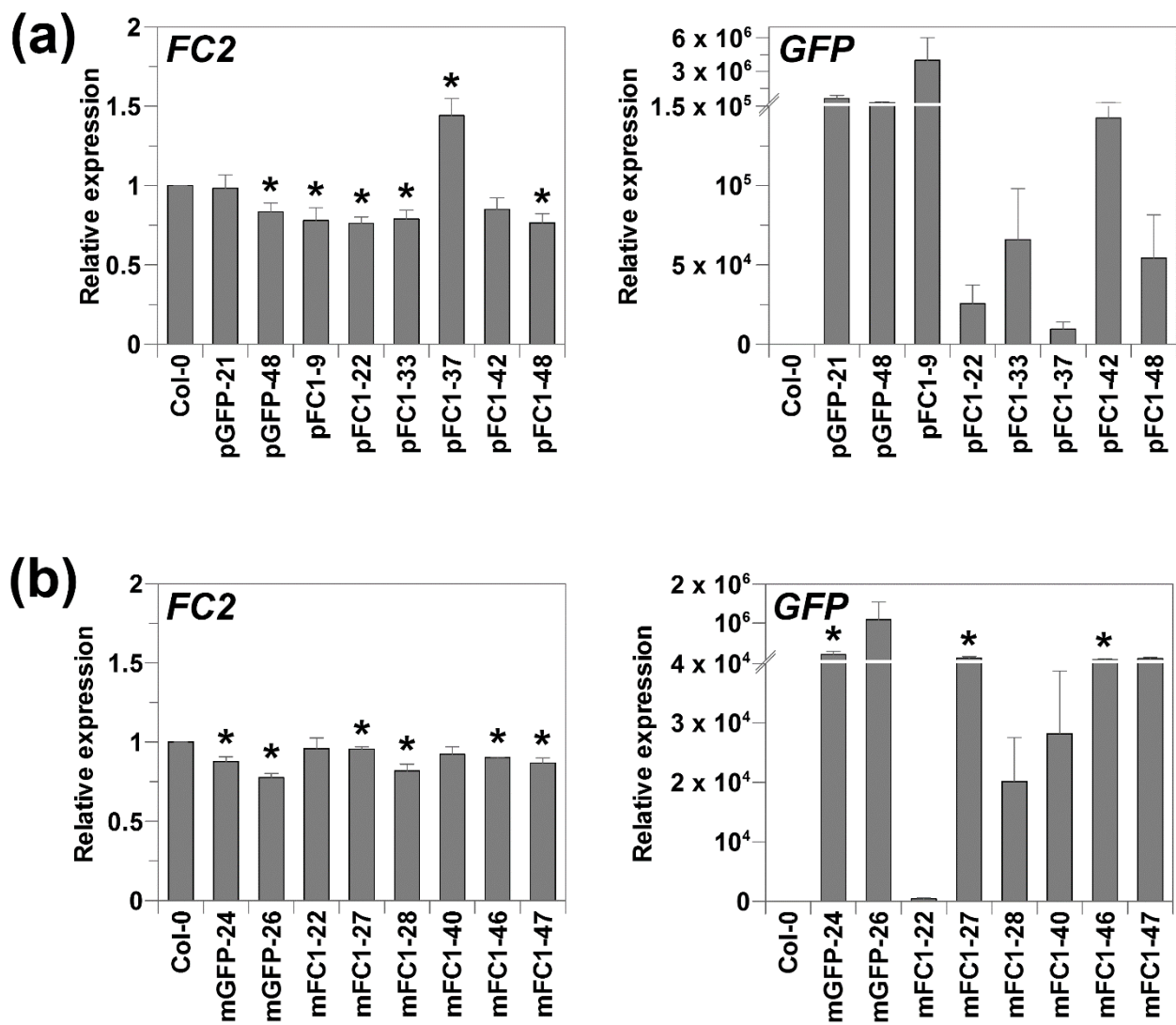


Figure S1. Expression of *FC2* and *GFP* in *FC1* overexpressing lines. (a,b) Expression of *FC2* and *GFP* was determined in the same pFC1 (a) and mFC1 (b) seedlings used to generate Figure 1 and is shown relative to Col-0. Lines expressing only *GFP* in plastids (pGFP) or mitochondria (mGFP) were included as controls. Data represents the mean + SEM of three independent biological replicates and asterisks indicate a significant difference vs. Col-0 ($p < 0.05$, Student's *t*-test).

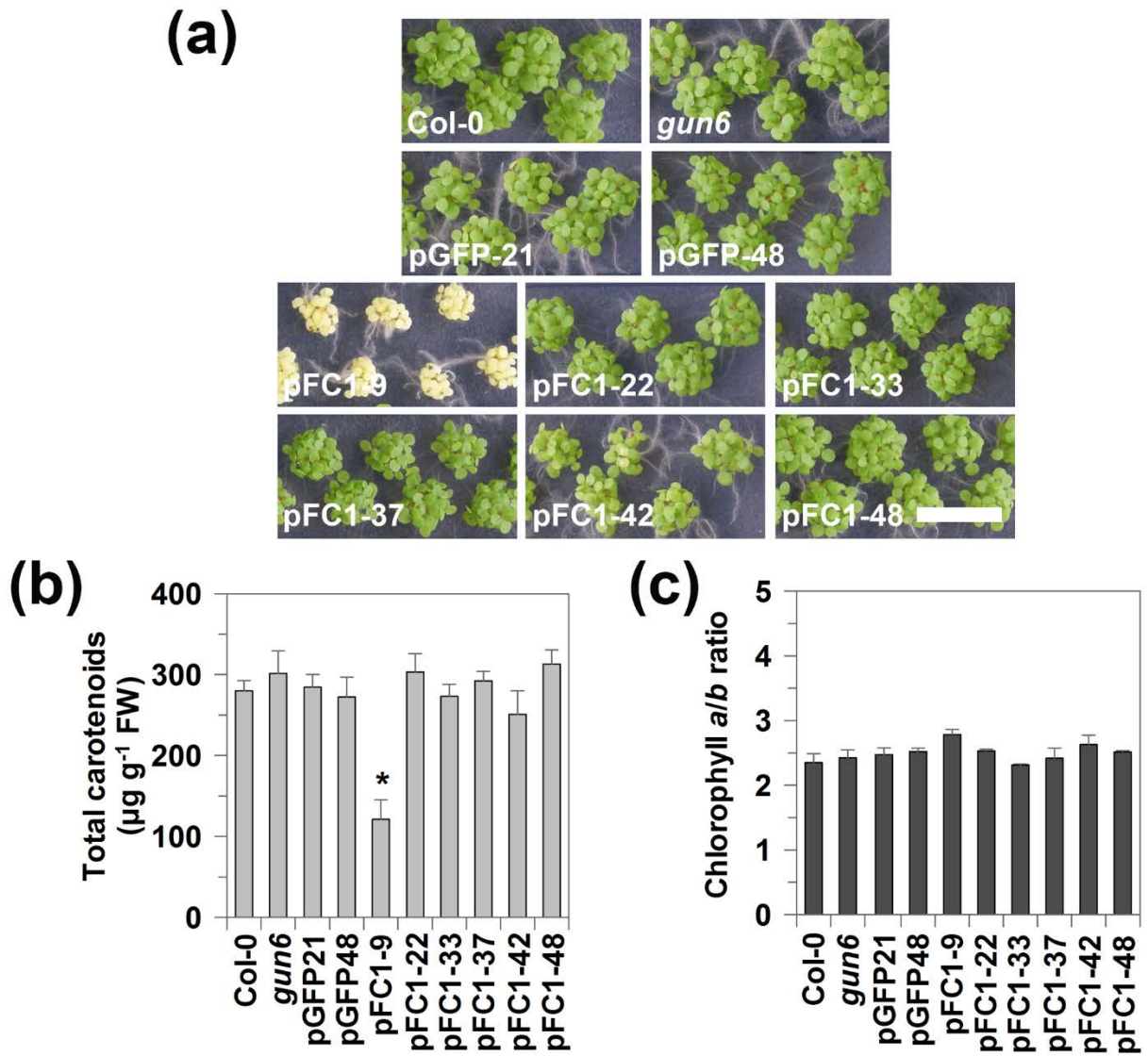


Figure S2. Characterisation of 5 day-old WLC-grown seedlings overexpressing plastid-targeted *FC1*. (a) Representative seedling phenotype of pFC1 and pGFP lines, bar = 10 mm. (b) Total carotenoid and (c) chlorophyll *a/b* ratio of the same transgenic lines. For (b, c), data shown is the mean + SEM of three independent biological replicates and the asterisk denotes a significant difference vs. Col-0 ($p < 0.05$, Student's *t*-test).

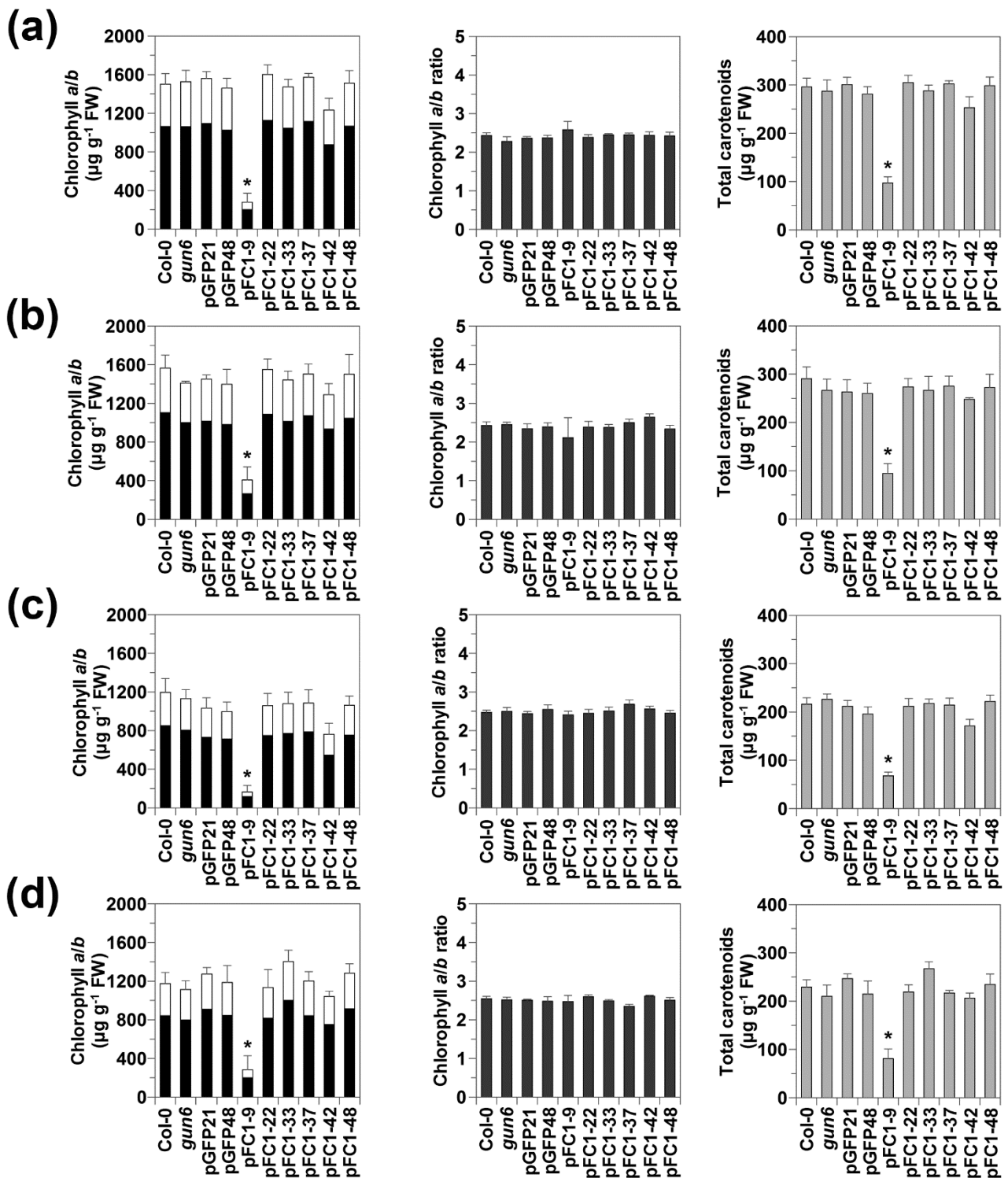


Figure S3. Analysis of chlorophyll and carotenoid levels in pFC1 seedlings grown in different light conditions. (a-d) Total chlorophyll, chlorophyll *a/b* ratio and total carotenoids were measured in pFC1, pGFP (control) and *gun6* 5 d-old seedlings under a range of conditions. (a) LWLc (25 $\mu\text{mol m}^{-2} \text{s}^{-1}$), (b) HWLc (250 $\mu\text{mol m}^{-2} \text{s}^{-1}$), (c) SD (8 h light, 16 h dark, 100 $\mu\text{mol m}^{-2} \text{s}^{-1}$), (d) LD (16 h light, 8 h dark, 100 $\mu\text{mol m}^{-2} \text{s}^{-1}$). For graphs of chlorophyll content, black bars represent chlorophyll *a* and white bars represent chlorophyll *b*. Data shown are the mean + SEM of three independent biological replicates and asterisks indicate a significant difference vs. Col-0 ($p < 0.05$, Student's *t*-test).

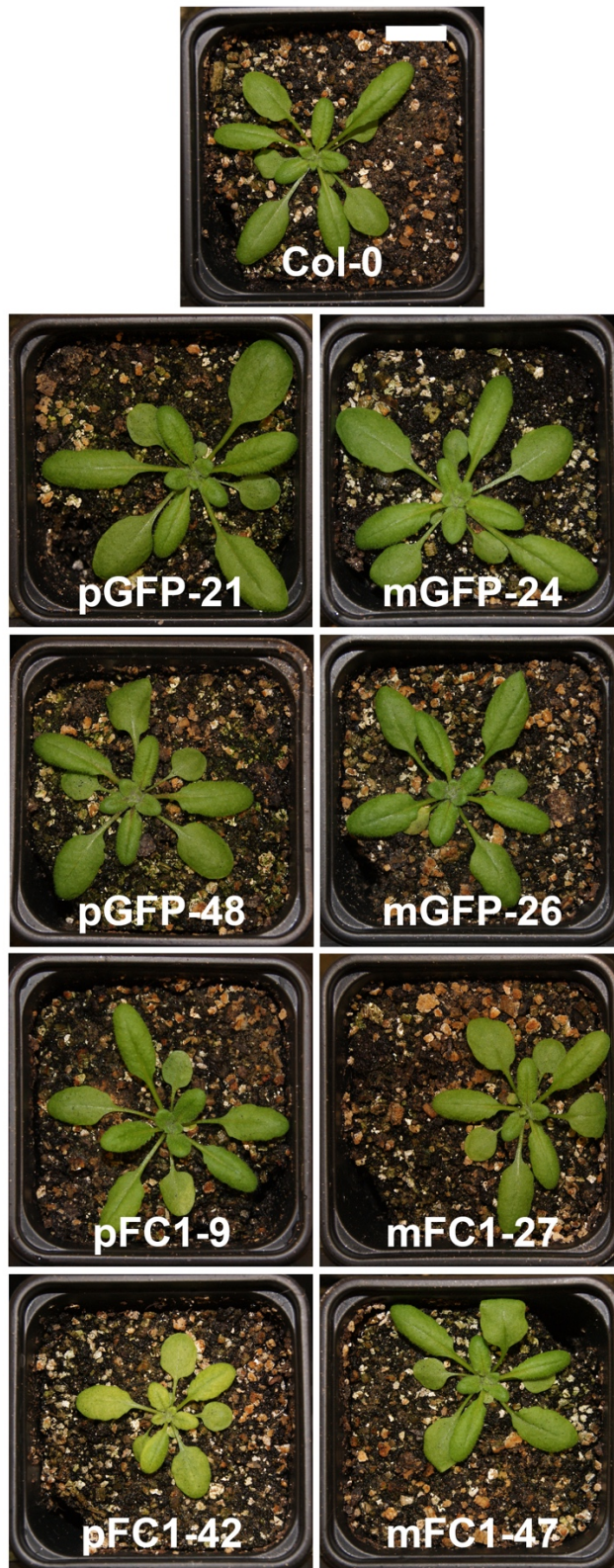


Figure S4. Phenotype of *FC1* overexpressing lines at the rosette stage. Representative photographs of pGFP, pFC1, mGFP and mFC1 lines. All photographs were taken 23 days after sowing (DAS), except pFC1-9 (34 DAS). Plants were grown on soil in LD conditions (16 h light, 8 h dark, $100 \mu\text{mol m}^{-2} \text{s}^{-1}$), scale bar = 10 mm.

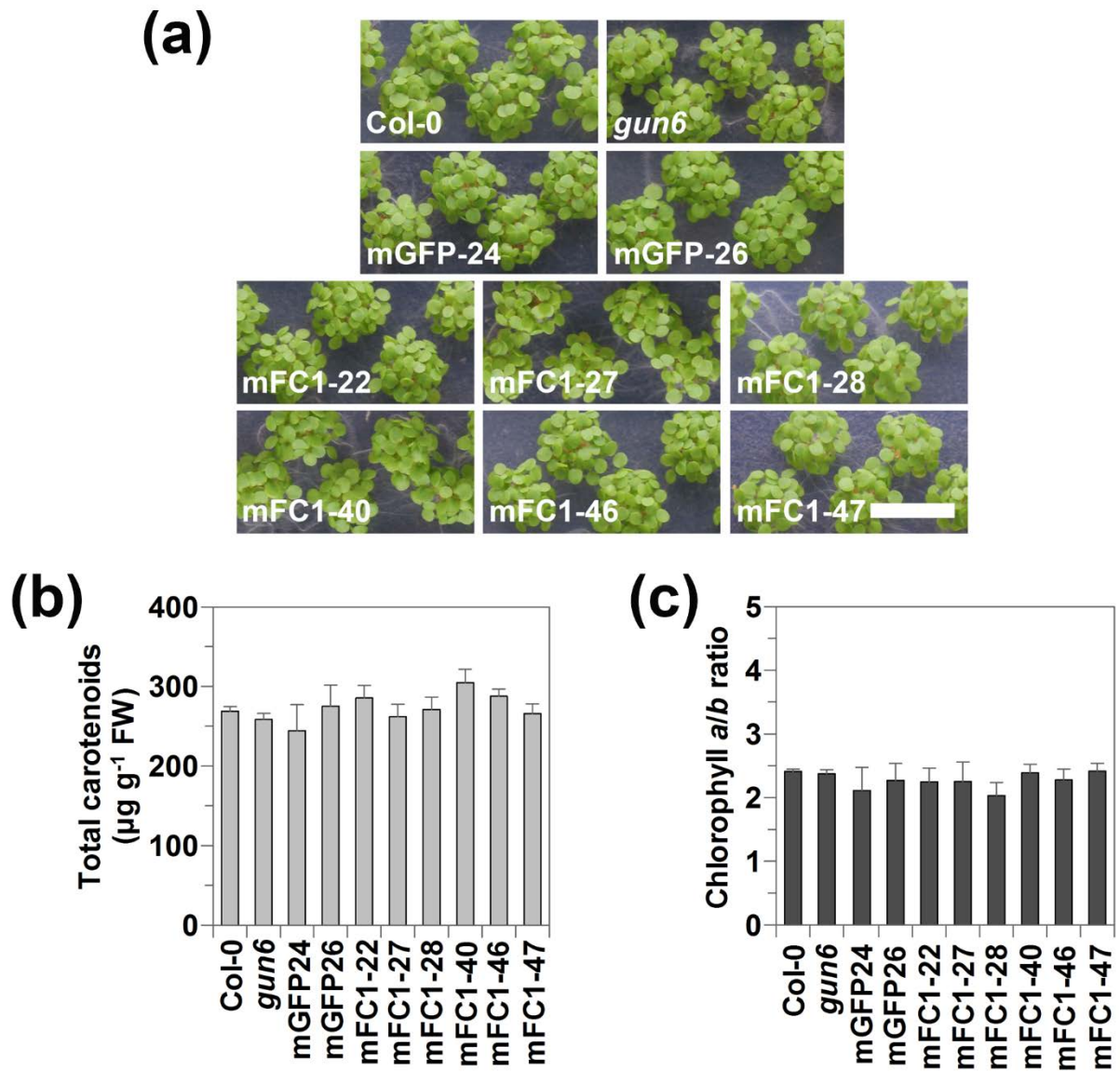


Figure S5. Characterisation of 5 d-old WLC-grown seedlings overexpressing mitochondria-targeted FC1. (a) Representative seedling phenotype of mFC1 and mGFP lines, bar = 10 mm. (b) Total carotenoid and (c) chlorophyll *a/b* ratio of the same transgenic lines. For (b) and (c), data shown is the mean + SEM of three independent biological replicates.

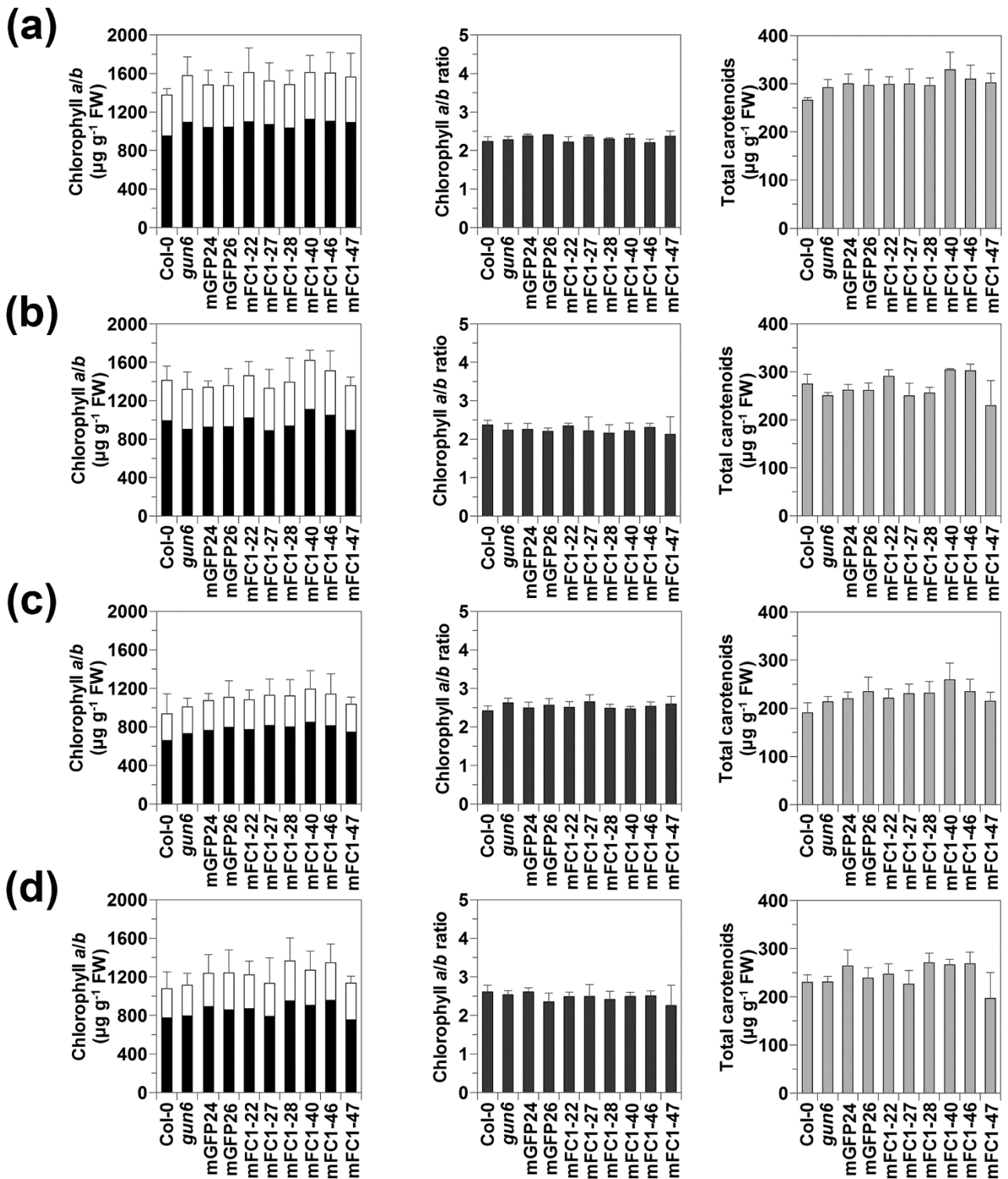


Figure S6. Analysis of chlorophyll and carotenoid levels in mFC1 seedlings grown in different light conditions. (a-d) Total chlorophyll, chlorophyll *a/b* ratio and total carotenoids were measured in mFC1, mGFP (control) and *gun6* 5 d-old seedlings under a range of conditions. (a) LWLc (25 µmol m⁻² s⁻¹), (b) HWLc (250 µmol m⁻² s⁻¹), (c) SD (8 h light, 16 h dark, 100 µmol m⁻² s⁻¹), (d) LD (16 h light, 8 h dark, 100 µmol m⁻² s⁻¹). For graphs of chlorophyll content, black bars represent chlorophyll *a* and white bars represent chlorophyll *b*. Data shown are the mean + SEM of three independent biological replicates.

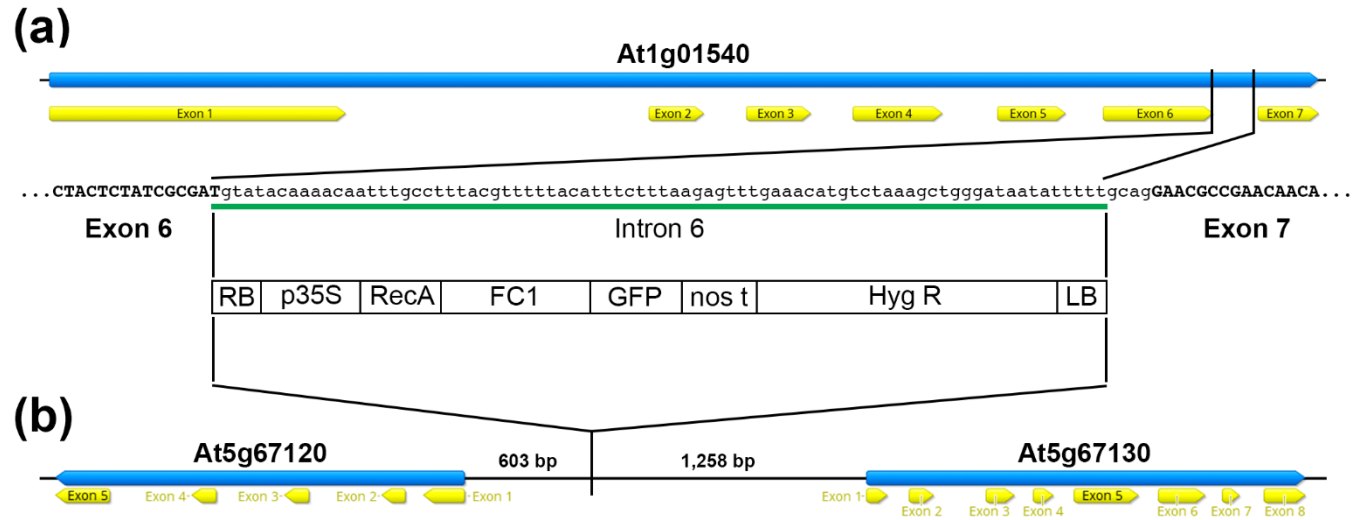


Figure S7. Insertion site of transgenic pFC1 cassettes. Diagram to show the insertion site of the transgenic cassette for (a) pFC1-9 and (b) pFC1-42. Exons (yellow boxes) are marked on the full-length genomic DNA sequence (blue boxes). The green line in (a) represents genomic sequence that has been replaced by the insertion. The base pair sizes in (b) give the distance from the insertion site to the start codon of each gene.

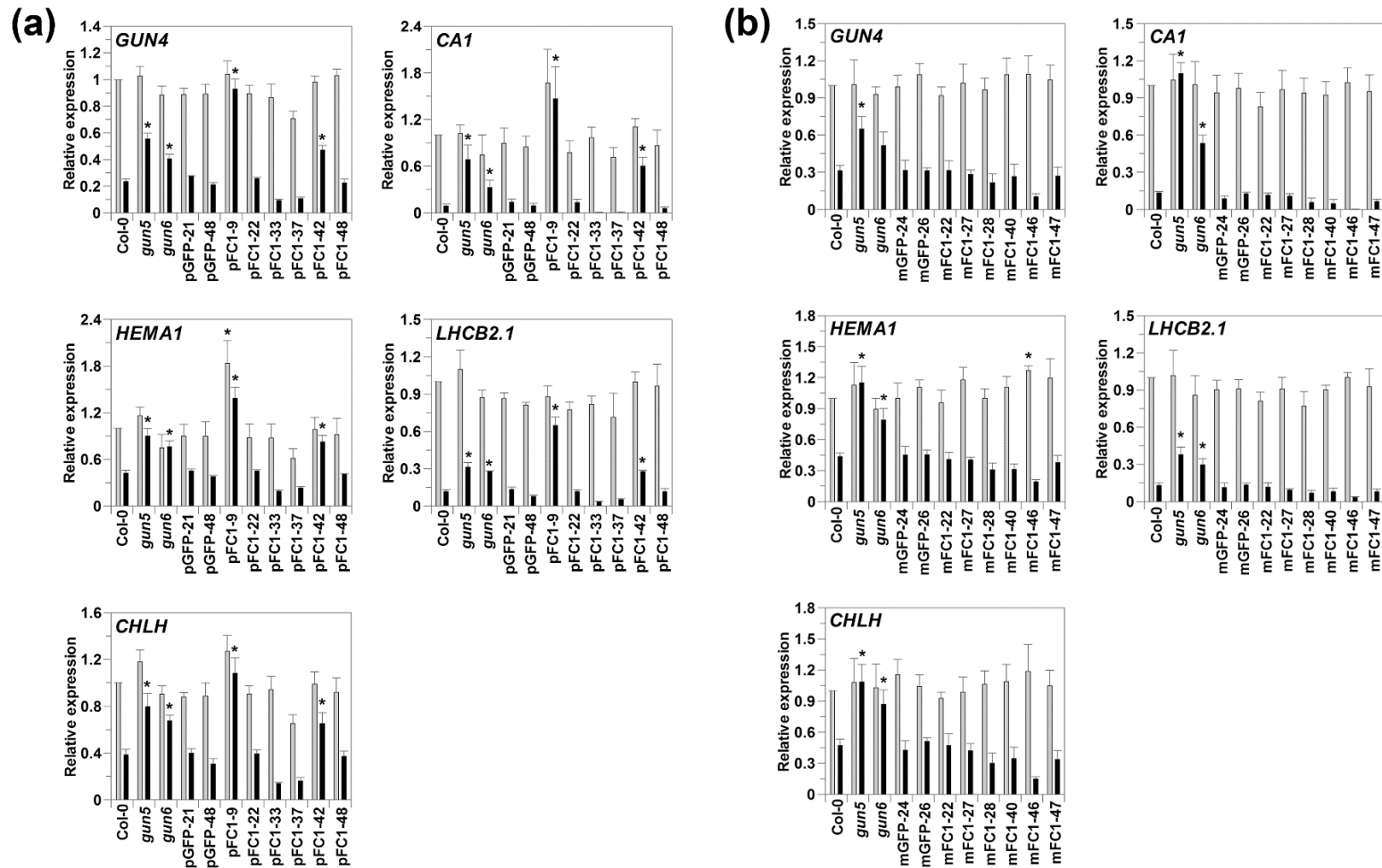


Figure S8. Expression of photosynthesis-associated genes on NF is rescued in plastid *FC1* overexpressors, but not mitochondrial *FC1* overexpressors. (a,b) The expression of *GUN4*, *CA1*, *HEMA1*, *LHCB2.1* and *CHLH* was determined by qRT-PCR in pFC1 (a) and mFC1 (b) seedlings grown for 7 d in LWLc on plates in the absence (grey bars) or presence (black bars) of NF. The control lines pGFP (a) and mGFP (b), as well as *gun5* and *gun6*, were included. Data shown are the mean fold changes vs. Col-0 on NF + SEM of three independent biological replicates and asterisks indicate a significant difference vs. Col-0 ($p < 0.05$, Student's *t*-test). The data in this figure was used to produce the graphs in Figure 3.

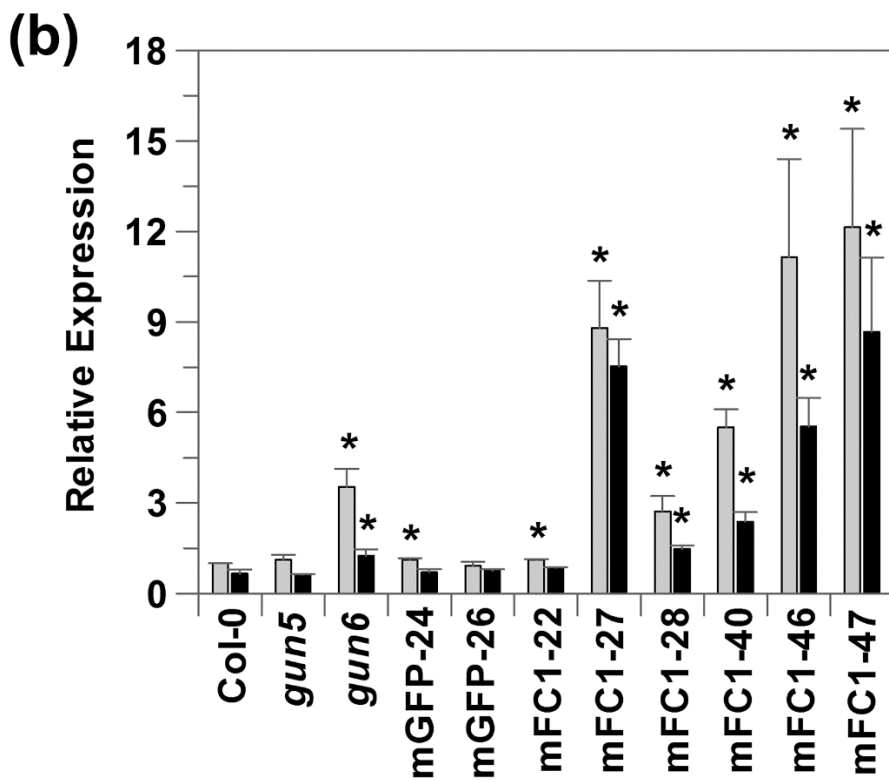
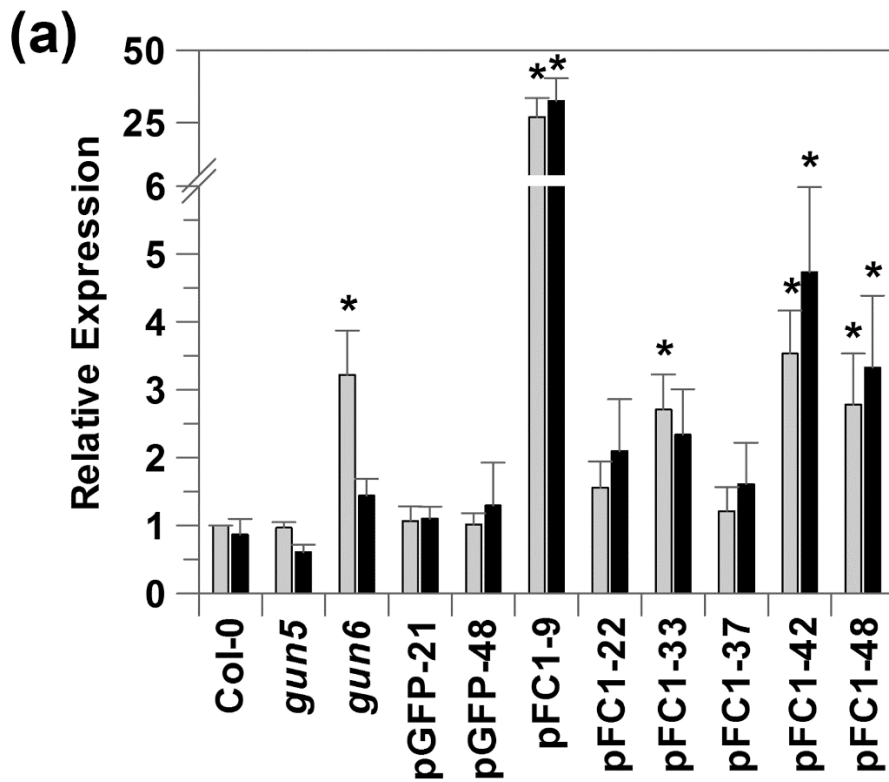


Figure S9. FC1 expression in pFC1 and mFC1 lines in the NF screen. (a,b) FC1 expression was determined by qRT-PCR in pFC1 (a) and mFC1 (b) seedlings in the absence (grey bars) or presence (black bars) of NF. Data represents the mean + SEM of three independent biological replicates and asterisks indicate a significant difference vs. Col-0 ($p < 0.05$, Student's *t*-test).

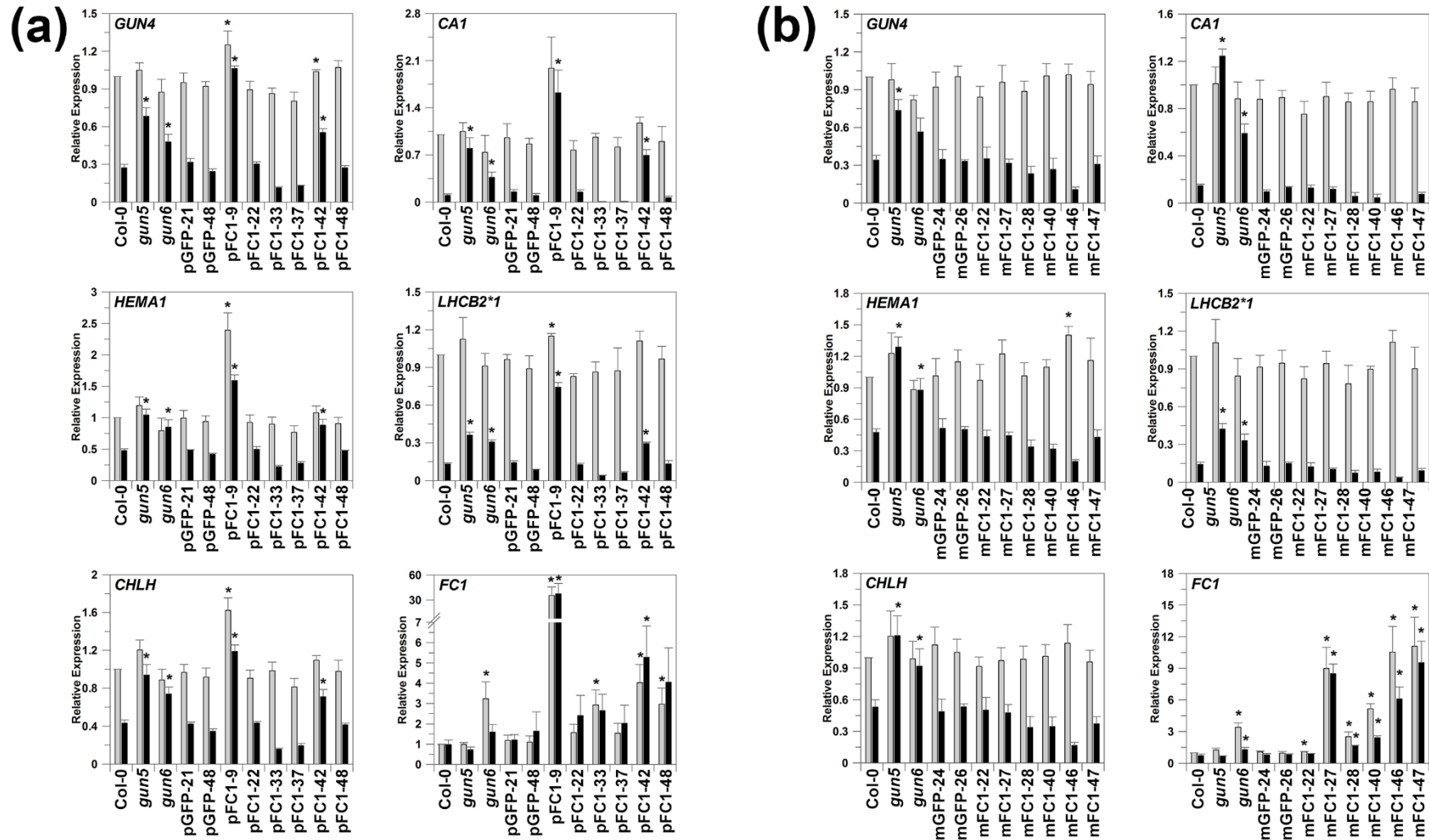


Figure S10. Gene expression changes on NF in pFC1 seedlings are not dependent on the qRT-PCR reference gene. (a,b) qRT-PCR data shown in electronic supplementary material figures S8 and S9 were normalised to a different reference gene, *YELLOW LEAF SPECIFIC GENE 8* (*YLS8*, At5g08290). The expression of *GUN4*, *CA1*, *HEMA1*, *LHCB2.1*, *CHLH* and *FC1* was determined by qRT-PCR in pFC1 (a) and mFC1(b) seedlings grown for 7 d in LWLc on plates in the absence (grey bars) or presence (black bars) of NF. The control lines pGFP (a) and mGFP (b), as well as *gun5* and *gun6*, were included. Data shown are the mean fold changes vs. Col-0 on NF + SEM of three independent biological replicates and asterisks indicate a significant difference vs. Col-0 ($p < 0.05$, Student's *t*-test).

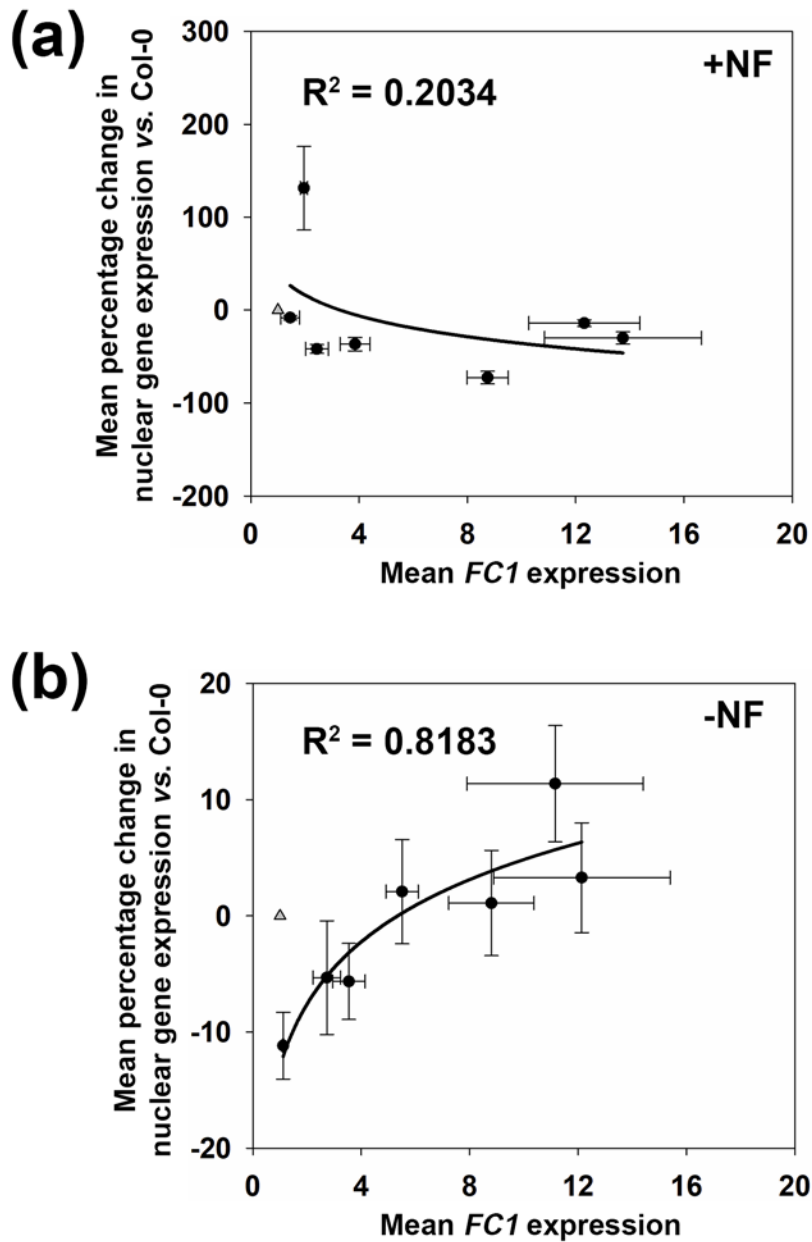


Figure S11. Mitochondria-targeted *FC1* expression does not correlate with enhanced nuclear gene expression on NF. Correlation plots of the combined mean percentage change in expression of *GUN4*, *CA1*, *HEMA1*, *LHCB2.1*, and *CHLH*, vs. *FC1* expression for m*FC1* seedlings in the presence (a) or absence (b) of NF. Data is relative to Col-0 +NF (a) or -NF (b). For both graphs, data points include *gun6* and the six transgenic m*FC1* overexpressing lines. The triangle indicates WT response. SigmaPlot 13.0 was used to fit logarithmic best-fit lines and derive coefficients of determination. Data shown is the mean \pm SEM of three independent biological replicates.

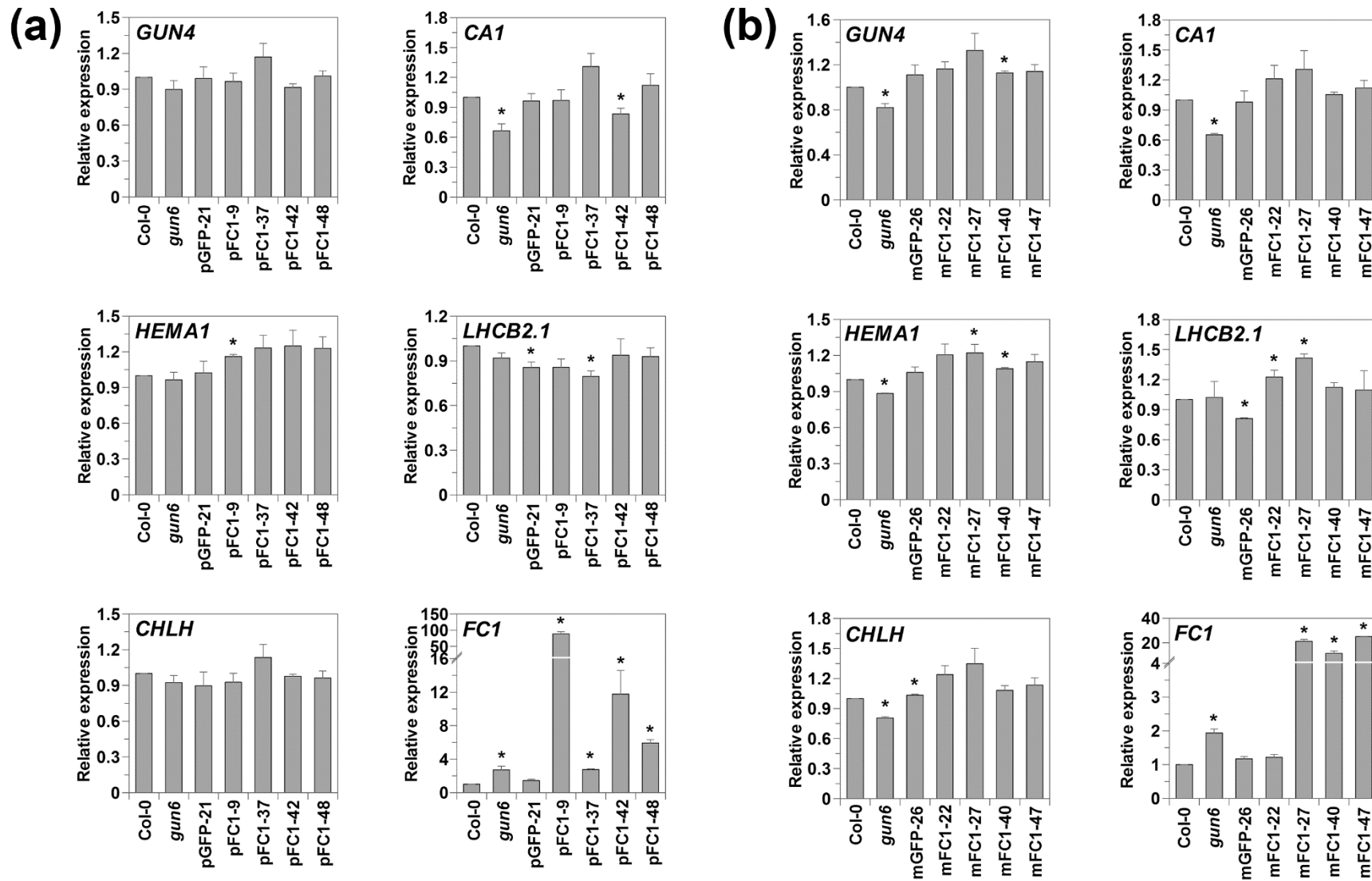


Figure S12. Increased *FC1* expression does not confer elevated nuclear gene expression in dark-grown seedlings. (a,b) The expression of *GUN4*, *CA1*, *HEMA1*, *LHCB2.1*, *CHLH* and *FC1* was determined by qRT-PCR in pFC1 (a) and mFC1 (b) seedlings grown for 4 d in the dark. Data shown is the mean + SEM of three independent biological replicates and asterisks denote a significant difference vs. Col-0 ($p < 0.05$, Student's *t*-test).

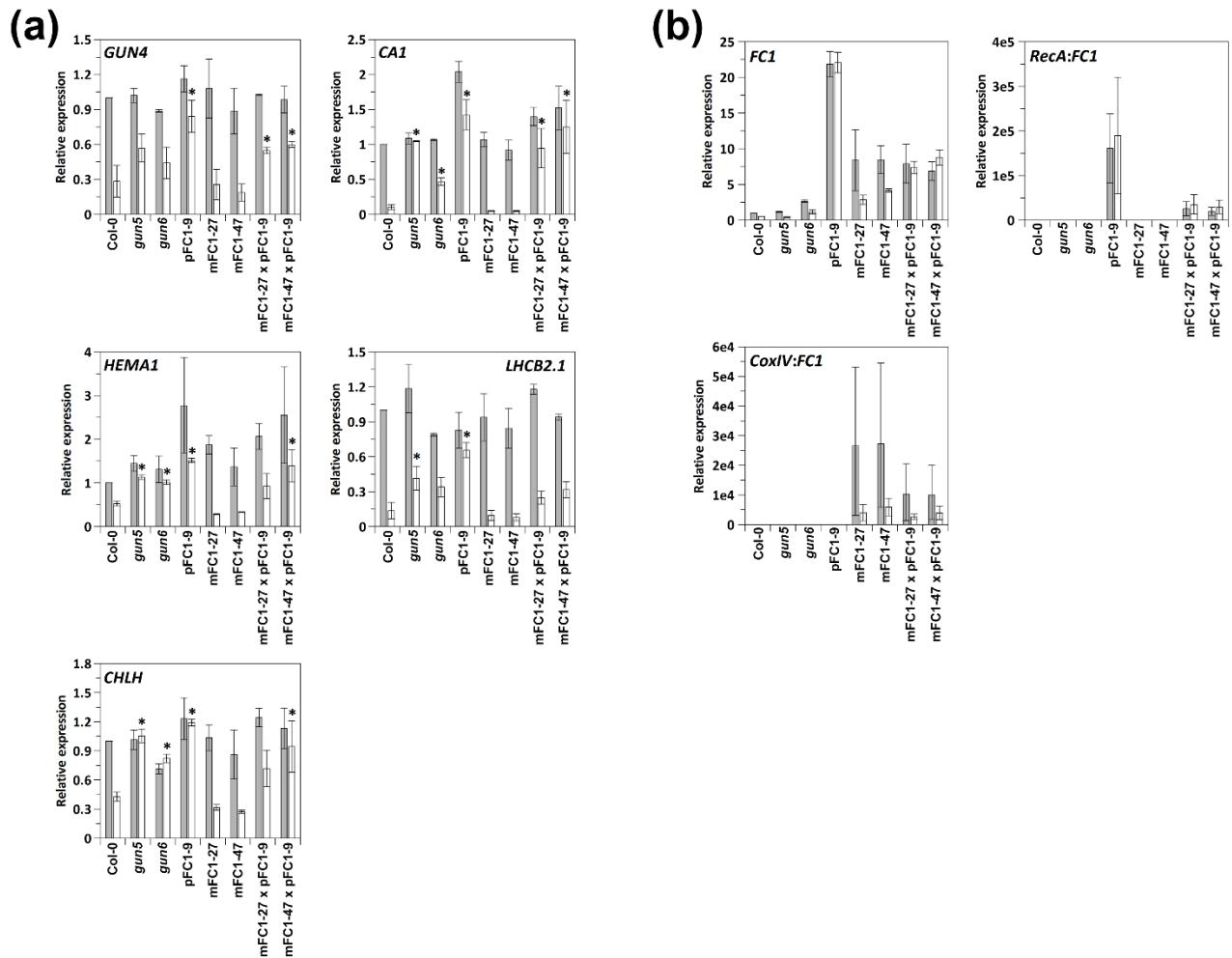


Figure S13. *FC1* overexpression in crosses of pFC1 and mFC1 transgenic lines. (a,b) Analysis of gene expression by qRT-PCR in F₁ seedlings derived from a cross between pFC1-9 and mFC1-27, or pFC1-9 and mFC1-47 was assessed in the absence (grey bars) or presence (white bars) of NF by qRT-PCR. The parent lines pFC1-9, mFC1-27 and mFC1-47, as-well-as *gun5* and *gun6*, were included as controls. Expression of *GUN4*, *CA1*, *HEMA1*, *LHC2.1* and *CHLH* (a) and total, plastid-targeted (*RecA:FC1*) and mitochondria-targeted (*CoxIV:FC1*) *FC1* (b) is shown relative to Col-0. Data shown is the mean \pm range of two independent biological replicates and asterisks denote a significant enhancement of nuclear gene expression vs. Col-0 +NF (determined as no overlap of the 95% confidence limits).

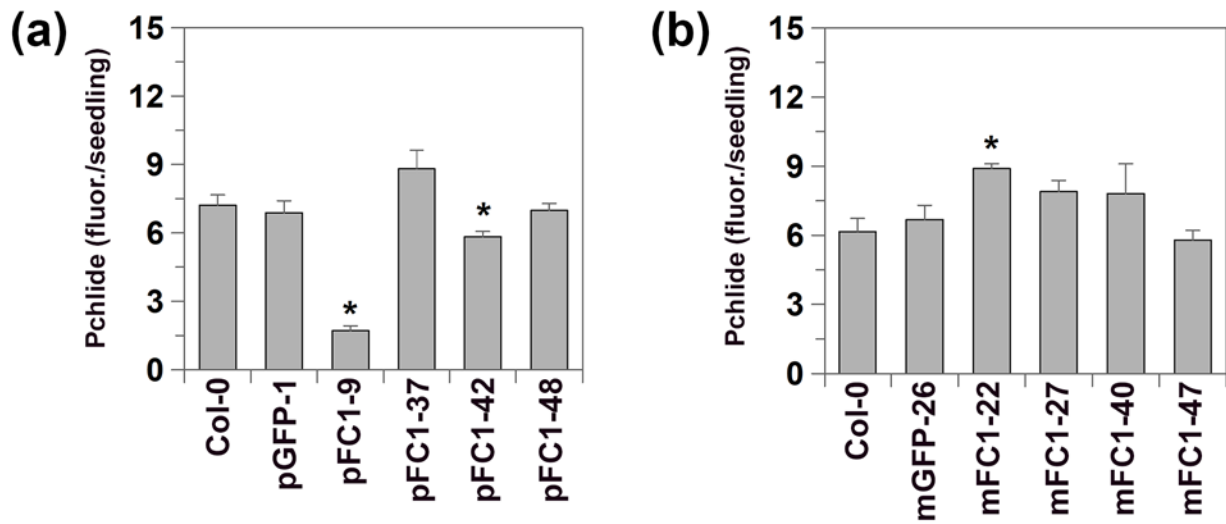


Figure S14. Protochlorophyllide is reduced in pFC1 lines. (a,b) Protochlorophyllide (Pchlide) content of pFC1 (a) and mFC1 (b) seedlings grown for 4 d in the dark. Data shown is the mean + SEM of three independent biological replicates and asterisks indicate a significant difference in percentage change vs. Col-0 for the same treatment (ANOVA, followed by Tukey's test).

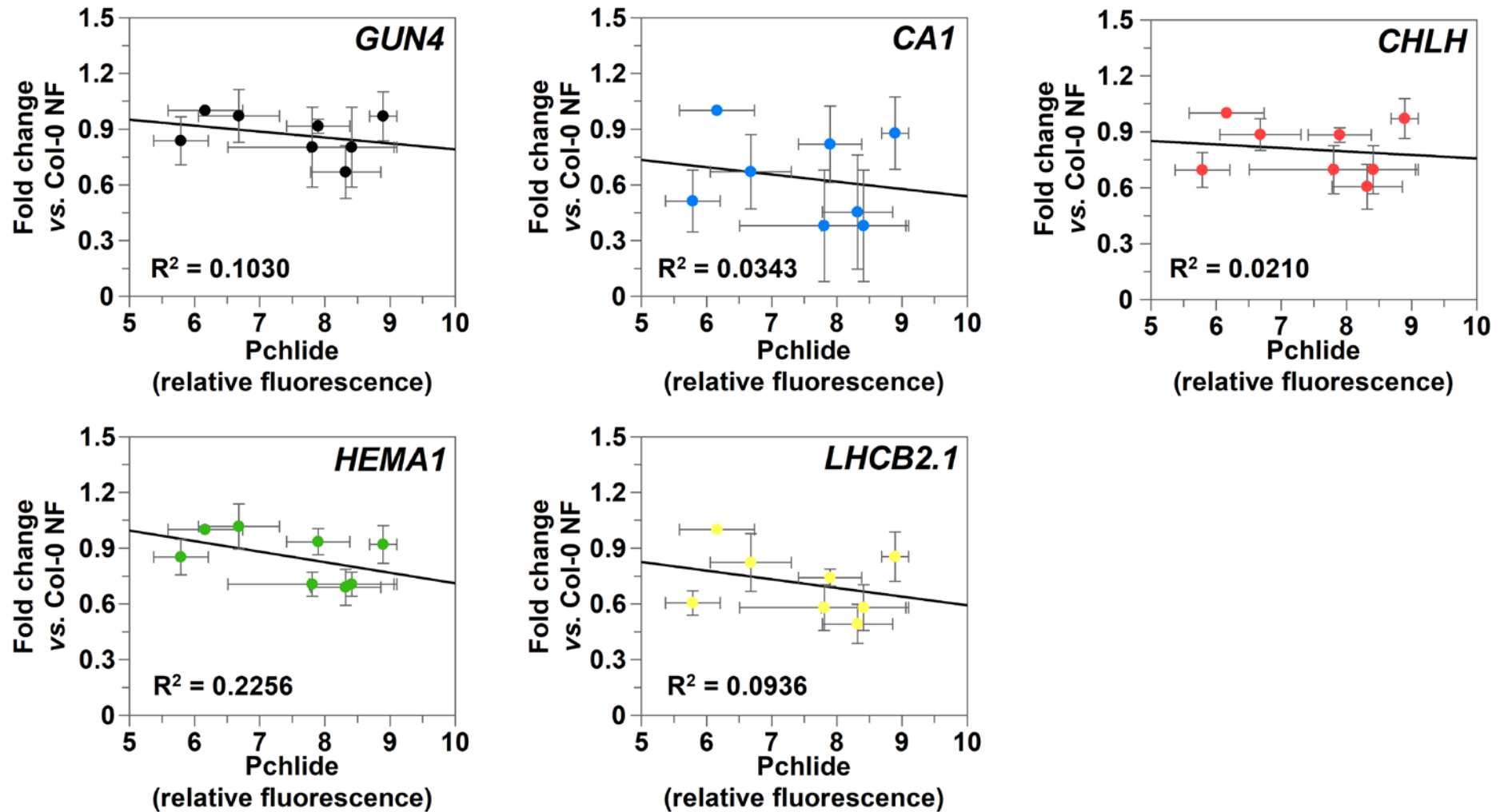


Figure S15. Enhancement of nuclear gene expression on NF does not correlate with protochlorophyllide levels in dark-grown mFC1 seedlings. Correlation plots of protochlorophyllide (Pchlide) in 4 d-old dark-grown mFC1 seedlings and against fold change in expression of *GUN4*, *CA1*, *HEMA1*, *LHCB2.1*, and *CHLH* vs. Col-0 on NF. Data represent the mean \pm SEM of three independent biological replicates.